NACA

RESEARCH MEMORANDUM

for the

Air Materiel Command, U. S. Air Force

WIND-TUNNEL INVESTIGATION OF THE LOW-SPEED STATIC STABILITY AND CONTROL CHARACTERISTICS OF A MODEL OF THE BELL MX-776 (RASCAL) IN COMBINED ANGLE OF ATTACK AND SIDESLIP

By William Letko

Langley Aeronautical Laboratory
Langley Field, Va.

NATIONAL ADVISORY COMMITTEE
FOR AERONAUTICS

WASHINGTON

APR 22 1952

NACA RM SL52D23

NATIONAL ADVISORY COMMITTEE FOR AERONAUTICS

RESEARCH MEMORANDUM

for the

Air Materiel Command, U. S. Air Force

WIND-TUNNEL INVESTIGATION OF THE LOW-SPEED STATIC STABILITY AND CONTROL CHARACTERISTICS OF A MODEL OF THE BELL MX-776 (RASCAL) IN COMBINED ANGLE OF ATTACK AND SIDESLIP

By William Letko

SUMMARY

An investigation has been made in the Langley stability tunnel to determine the low-speed static stability and control characteristics of a model of the Bell MX-776. The results show the model to be longitudinally unstable in the angle-of-attack range around zero angle of attack and to become stable at moderate angles of attack. The results of the present investigation agree reasonably well with results obtained in other facilities at low speed. The present pitching-moment results at low Mach numbers also agree reasonably well with unpublished results of tests of the model at supersonic Mach numbers (up to Mach number 1.86). Unpublished results at moderate and high subsonic speeds, however, indicate considerably greater instability at low angles of attack than is indicated by low-speed results. The results of the present tests also showed that the pitching-moment coefficients for angles of attack up to 12° remained fairly constant with sideslip angle up to 12°.

The elevators tested produced relatively large pitching moments at zero angle of attack but, as the angle of attack was increased, the elevator effectiveness decreased. The rate of decrease of elevator effectiveness with angle of attack was less for 8° than for 20° elevator deflection. Therefore although 8° deflection caused an appreciable change in longitudinal trim angle and trim lift coefficient a deflection of 20° caused only a small additional increase in trim angle and trim lift coefficient.

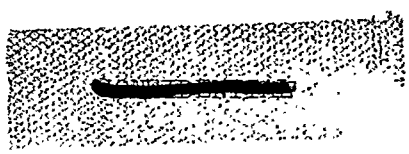

The variation of yawing-moment coefficient with sideslip angle was nonlinear, and the complete model was about neutrally stable in the sideslip range near zero sideslip angle for low and medium angles of attack.

INTRODUCTION

The aerodynamic characteristics of the latest version of the MX-776 missile were studied in 1951 at Wright-Patterson Air Force Base, Ohio at a Mach number of 0.13 and a Reynolds number (based on maximum body diameter) of about 287,000 and in the blowdown tunnel at the Naval Ordnance Laboratory, Silver Springs, Maryland at Mach numbers from 0.20 to 1.86. The Reynolds number for the test in the blowdown tunnel at 0.20 Mach number was about 160,000. Because of some uncertainty concerning the tare corrections for the low-speed data and because of the large aerodynamic nonlinearities and interference effects in combined pitch and sideslip indicated by previous tests of an earlier version of this missile in the Langley stability tunnel (ref. 1), a low-speed investigation was made in the Langley stability tunnel to obtain a check on the low-speed data and to investigate the characteristics of the model in combined pitch and sideslip. The results of this investigation are presented herein.

SYMBOLS AND COEFFICIENTS

All forces and moments are given with respect to the system of wind axes shown in figure 1. The origin of the axes is located at a point which corresponds to the center of gravity of the missile. The symbols and coefficients used herein are defined as follows:

C_L	lift coefficient, L/qS_F
C_D	drag coefficient, D/qS_F
C_Y	side-force coefficient, Y/qS_F
C_m	pitching-moment coefficient, $M/qS_F\ d$
C_l	rolling-moment coefficient, $L'/qS_F\ d$
C_n	yawing-moment coefficient, $N/qS_F\ d$
L	lift, lb

D	drag, lb
Y	side force, lb
M	pitching moment, ft-lb
L'	rolling moment, ft-lb
N	yawing moment, ft-lb
q	dynamic pressure, $\rho V^2/2$, lb/sq ft
ρ	mass density, slugs/cu ft
V	free-stream velocity, ft/sec
M	Mach number
S_F	model body frontal area (0.349 sq ft)
d	maximum diameter of model body (0.667 ft)
$\bar{c}$	mean aerodynamic chord, ft
α	angle of attack of body center line, deg
β	angle of sideslip of body center line, deg
δ_e	elevator deflection, positive when trailing edge is down, deg
δ_{FV}	deflection of all-movable forward vertical surface, positive trailing edge to left, deg

APPARATUS AND MODELS

The tests of this investigation were made in the 6- by 6-foot test section of the Langley stability tunnel. The model used was one of the $\frac{1}{6}$-scale models provided the National Advisory Committee for Aeronautics for flight tests at the Pilotless Aircraft Research Station, Wallops Island, Va. A sketch showing the general arrangement of the model is given as figure 2 and table I gives the general specifications of the model. The body of the model was made of balsa wood with aluminum castings to serve as mounts for the horizontal and vertical surfaces. In order to adapt the model for balance tests, a steel tube was inserted

in the body of the model and bolted to a single-strut support which was fastened to a six-component balance system. A photograph of the model in the Langley stability tunnel test section is given as figure 3.

All model surfaces were machined of dural. For these tests, the metal ailerons on the rear wing were replaced by ones made of wood. Variations of circular-arc airfoil sections were used for all model surfaces. True symmetrical circular-arc airfoils were used for both sets of fins in the vertical plane with maximum thickness ratios varying from 3 percent at the tips to 5.4 percent at the fuselage center line. For these tests, the forward vertical fin was modified to allow deflection as an all-movable surface about an axis perpendicular to the body axis and passing through the point of interesection of the 50-percent-chord line and the body surface. The forward horizontal wing was of symmetrical circular-arc airfoil section ahead of the 75-percent-chord station with straight lines from there to the trailing edge to give a section with the trailing-edge thickness equal to one-half of that at the 75-percent-chord location. The maximum thickness ratio varied from 3 percent at the tips to 5.2 percent at the model center line. The forward horizontal surfaces were cut along the 75-percent-chord line for these tests to give 25-percent-chord elevators. The elevator angles were set by the use of thin metal brackets bent to give desired elevator deflections. These brackets also served as seals between the wing and elevator. An airfoil similar to that of the forward horizontal surface was used for the rear horizontal surface but this surface had a constant thickness behind the 75-percent-chord station so that a sealed, full-slab control surface resulted as shown in section view in figure 2. For these tests, the original deflected metal full-slab control surfaces were replaced by ones made of wood. They were not deflected for any of the present tests. The maximum thickness ratio of the rear horizontal surface varied from 4 percent at the tip to 6.2 percent at the model center line.

TESTS

Most of the tests were made at a dynamic pressure of 24.9 pounds per square foot which corresponds to a Mach number of 0.13 and a Reynolds number based on maximum body diameter of about 625,000 (sea-level conditions). The longitudinal characteristics of the complete model were also determined at a dynamic pressure of 98.3 pounds per square foot which corresponds to a Mach number of 0.26 and a Reynolds number of about 1,330,000.

The model was tested through an angle-of-attack range from about -4° to about 28° angle of attack for zero and $\pm 4^\circ$ angle of sideslip.

Tests were also made through a range of sideslip angles from about -24° to about 12° for several angles of attack, and the complete model was tested through a greater range of angles of attack than were other configurations. Some of the other configurations tested were: model with forward horizontal surfaces off, forward vertical surfaces off and both forward surfaces off. Similar tests were also made for the complete model with several deflections of the forward vertical surface and for the complete model for several elevator deflections. A list of the configurations investigated is presented in table II.

The data were measured about a point located 34 inches from the nose of the model but the data were computed and are presented about a point located 38.167 inches from the nose of the model which corresponds to the center of gravity at which the full-scale missile is fired.

CORRECTIONS

Corrections were applied for support-strut interference to all data where the angle of attack varied and the angle of sideslip remained constant. However, no support-strut corrections were applied to those angle-of-attack runs for which the angle of sideslip exceeded ±4°. The pitching and yawing moments were corrected in all tests for the jet-boundary effects (determined by use of ref. 2) in a manner similar to that of reference 1. These corrections which were added to the calculated coefficients are given in the following table:

Horizontal surfaces		Vertical surfaces		$\Delta C_m = K_1\alpha$	$\Delta C_n = -K_2\beta$
Front	Rear	Front	Rear	K_1	K_2
On	On	On	On	0.0420	0.0108
Off	On	On	On	.0279	.0108
Off	On	Off	On	.0279	.0080
On	On	Off	On	.0420	.0080

The angles of attack and of yaw were corrected for deflections of the model support strut.

RESULTS AND DISCUSSION

Presentation of Results

The static longitudinal stability and control characteristics are presented in figures 4 to 10. The static lateral and directional characteristics and directional control characteristics are shown in figures 11 to 14. Table II is a list of the configurations investigated with a list of figures which contain data related to each configuration.

Longitudinal Characteristics

Stability.- The longitudinal characteristics of the complete model are shown in figure 4 for Mach numbers of 0.13 and 0.26. The data show that the model is unstable in the angle-of-attack range near zero angle of attack and becomes stable at moderate angles of attack above about 4°. The nonlinearity near zero angle of attack can be largely attributed to downwash as was indicated in reference 1 which presents the results of tests of an earlier version of the missile. The figure also shows that increasing the Mach number from 0.13 to 0.26 had very little effect on the stability in the low angle-of-attack range.

As was mentioned previously, the model was tested in other facilities and the pitching-moment data as obtained from unpublished preliminary-data plots is presented in figure 5 for Mach numbers of 0.13, 0.60, and 1.28. For comparison, the pitching-moment data of the present investigation for Mach number of 0.13 are also presented in the figure. From the figure, it can be seen that the data at Mach number 0.13 from both investigations agrees reasonably well around zero angle of attack. The data for Mach number 0.60 show a rather large increase in instability over that obtained at Mach number 0.13. For Mach number 1.28, however, the data show a decrease in instability and the variation of pitching-moment coefficients with angle of attack is very nearly the same as that obtained in the present investigation for Mach number 0.13. Data (not presented) show less variation of stability with Mach number in the range above Mach number 1.0 than for subsonic Mach numbers and fairly good agreement with the Mach number 0.13 data was indicated for Mach numbers as high as 1.86. This behavior is not unexpected, however, because low-aspect-ratio surfaces, in general, have similar aerodynamic characteristics at low subsonic and supersonic speeds.

The data of figure 6 show that small angles of sideslip had only small effects on the variation of lift, drag, and pitching moment with angle of attack. The effects of larger sideslip angles on lift, drag, and pitching-moment coefficients of the model can be seen from figure 7

which presents the variation of these coefficients with angle of sideslip for constant angles of attack. The lift and pitching-moment coefficients were fairly constant with sideslip angle for angles of sideslip up to about 12°. This was true up to angles of attack of 12°; however, above 12° angle of attack, some stalling of the surfaces occurred and the lift and pitching moment varied irregularly with angle of sideslip.

The variation of lift, drag, and pitching-moment coefficients with angle of attack (Mach number of 0.13) is presented in figure 8 for the model with the forward horizontal surfaces removed. From a comparison of figure 8 and figure 4, it can be seen that removing the forward horizontal surface results in a stable pitching-moment variation through the greater part of the angle-of-attack range as was expected. There is a slight "hitch" in the lift and pitching-moment curves near zero angle of attack which was observed in other investigations of this missile. This hitch is believed to be caused either by the slab trailing edge of the rear surface or results from mutual interference between the body and the surface.

Control.- The effects of elevator deflection on C_L, C_D, and C_m are shown in figure 9. Deflecting the elevators causes a small increase in drag at low angles of attack as was expected. The increase in drag caused by elevators becomes larger as the angle of attack is increased. The effects of elevator deflection on C_L and C_m are similar with the effect on C_m being more pronounced. Elevator deflections caused a relatively large and generally linear increase in C_L and C_m in the range around zero angle of attack but the effectiveness of the elevators decreased as the angle of attack approached the angle of stall. The rate of decrease of elevator effectiveness with angle of attack was less for 8° deflection than for 20°. Therefore, although the 8° deflection caused a 5° increase in trim angle and an increase of 2.5 in trim lift coefficient, a deflection of 20° resulted in an additional increase in trim angle of only 1° and a negligible increase in trim lift coefficient.

The effects of sideslip angle on the elevator characteristics can be seen in figure 10 for the model with elevator deflected 8°. The increase in lift and drag coefficients with sideslip angle are similar to those obtained with the elevators undeflected. The most important characteristic to be noted is the change in longitudinal trim angle caused by the change in angle of sideslip. However, even though the change in sideslip angle from -8° to -20° caused a change in trim angle of about 5° from 11.5 to 16.8, the change in lift coefficient was comparatively small (from 6.8 to 7.7) because stall of the model occurred at about 12° angle of attack.

Lateral and Directional Characteristics

Stability.- The lateral and directional static stability characteristics of the normal configuration at various angles of attack are given in figure 11. Figure 11 shows that the slope of the curve of C_l against β is zero for zero angle of attack and small sideslip angles. The slope is slightly negative at other angles of attack up to about 16° but the range of sideslip angles for which the slope is negative at 16° angle of attack is small. At higher angles of attack, the slope (C_l against β) is positive for small and medium angles of sideslip. The variation of C_n with sideslip angle is nonlinear with the directional stability being almost neutral for low angles of attack and small sideslip angles. This nonlinearity can be attributed largely to the nonlinear directional characteristics of the body alone and partly to the sidewash from the forward vertical surfaces. Unpublished data show that the body alone has nonlinear directional characteristics at zero angle of attack. Asymmetry in the data at high angles of attack as evidenced by the curves of C_l and C_n against β (fig. 11) can be attributed to asymmetrical stall of the model surfaces.

The variations of C_l, C_n, and C_Y with sideslip angle for the model with elevators deflected 8° and 20° are presented in figure 12. From this figure, it can be seen that there are only small effects of elevator deflection on the lateral and directional characteristics of the model for the angles of attack presented.

A comparison of the variation of yawing moment, rolling moment, and side-force coefficient with angle of sideslip of the basic model and the model with different forward surfaces removed is presented in figure 13. Removing the forward vertical surface increases the directional stability for most of the angles of sideslip tested for all angles of attack. Again the nonlinearity of the curve of C_n against β at low angles of attack can be attributed to the nonlinear directional characteristics of the body alone. Removing only the forward horizontal surfaces generally causes small changes in C_Y, C_n, and C_l at small angles of attack and small angles of sideslip probably because of changes in sidewash and other interference effects. These changes become larger at higher angles of attack and sideslip. Removing all the forward surfaces of the model generally increases the directional stability of the model, the effect varying irregularly with angle of attack.

Control.- No lateral control (aileron) tests were made and only brief directional control tests were made, the results of which are presented in figure 14. The data show that deflection of the forward

vertical surfaces from 0° to 8° caused an appreciable change in sideslip trim angle, but additional deflection to 20° did not increase the sideslip trim angle over that obtained for 8° deflection for the angles of attack investigated.

CONCLUSIONS

The results of tests made to determine the low-speed static stability and control characteristics of a model of the Bell MX-776 (Rascal) have led to the following conclusions:

1. The data show the model to be longitudinally unstable in the angle-of-attack range around zero angle of attack and to become stable at moderate angles of attack. The longitudinal stability results of the present investigation agree reasonably well with results at low speeds of other facilities.

2. The present pitching-moment results at a low Mach number agree reasonably well with unpublished results of tests of the model at supersonic Mach numbers (up to Mach number 1.86). Unpublished results at moderate and high subsonic speeds, however, indicate considerably greater instability at low angles than is indicated by the present low-speed results.

3. The pitching-moment coefficients for angles of attack up to 12° remained fairly constant with sideslip angle up to 12°.

4. The elevators produced relatively large pitching moments at zero angle of attack but as the angle of attack increased the elevator effectiveness decreased. The rate of decrease of elevator effectiveness with angle of attack was less for 8° than for 20° elevator deflection. Therefore, although 8° deflection caused an appreciable change in longitudinal trim angle and trim lift coefficient a deflection of 20° caused only a small additional increase in trim angle and trim lift coefficient.

5. The variation of yawing-moment coefficient with sideslip angle was nonlinear, and the complete model was about neutrally stable in the sideslip range near zero sideslip angle for low and medium angles of attack.

Langley Aeronautical Laboratory
National Advisory Committee for Aeronautics
Langley Field, Va.

William Letko
William Letko
Aeronautical Research Scientist

Approved: Thomas A. Harris.
Thomas A. Harris
Chief of Stability Research Division

VR

REFERENCES

1. Queijo, M. J., and Michael, W. H., Jr.: Wind-Tunnel Investigation of the Low-Speed Static Stability and Control Characteristics of a Model of Bell MX-776. NACA RM SL9G08, U. S. Air Force, 1949.

2. Silverstein, Abe, and White, James A.: Wind-Tunnel Interference with Particular Reference to Off-Center Positions of the Wing and to the Downwash at the Tail. NACA Rep. 547, 1936.

TABLE I

GENERAL SPECIFICATIONS

[Fuselage: Over-all length, 64.00 in.; maximum diameter, 8.00 in.]

	Rear horizontal surfaces	Forward horizontal surfaces	Rear vertical surfaces	Forward vertical surfaces
Aspect ratio	3.05	3.22	3.20	3.70
Total span, in.	33.42	22.90	25.00	13.27
Total area, sq ft	2.54	1.13	1.36	0.33
Angle of incidence, deg	0	0	0	0
Dihedral, deg	0	0	0	0
Sweep, 0.75-chord, deg	0	0	0	0
Root chord at model center line, c_r, in.	17.11	11.36	12.45	6.03
Tip chord, c_t, in.	4.78	2.87	3.19	1.13
Root thickness ratio, t_r/c_r	0.062	0.052	0.052	0.054
Tip thickness ratio, t_t/c_t	0.040	0.030	0.030	0.030
Hinge-line location, percent chord	75.0	75.00		(a)
Airfoil section	(b)	(c)	(d)	(d)

[a]Hinge line is perpendicular to body axis and passes through the point of intersection of the 50-percent-chord line and the body surface

[b]Symmetrical circular arc with full-slab behind 75-percent chord

[c]Symmetrical circular arc with half-slab behind 75-percent chord

[d]Symmetrical circular arc

TABLE II

CONFIGURATIONS INVESTIGATED AND LIST OF PERTINENT FIGURES

Configuration				δ_e	δ_{FV}	Characteristics shown	Figure
Horizontal surfaces		Vertical surfaces					
Front	Rear	Front	Rear				
On	On	On	On	0	0	Longitudinal	4
On	On	On	On	0	0	Longitudinal	5
On	On	On	On	0	0	Longitudinal	6
On	On	On	On	0	0	Longitudinal	7
Off	On	On	On		0	Longitudinal	8
On	On	On	On	0,8,20	0	Longitudinal	9
On	On	On	On	8	0	Longitudinal	10
On	On	On	On	0	0	Lateral and directional	11
On	On	On	On	0,8,20	0	Lateral and directional	12
On	On	On	On	0	0	Lateral and directional	13
Off	On	On	On		0	Lateral and directional	13
On	On	Off	On	0		Lateral and directional	13
Off	On	Off	On			Lateral and directional	13
On	On	On	On	0	0,8,20	Lateral and directional	14

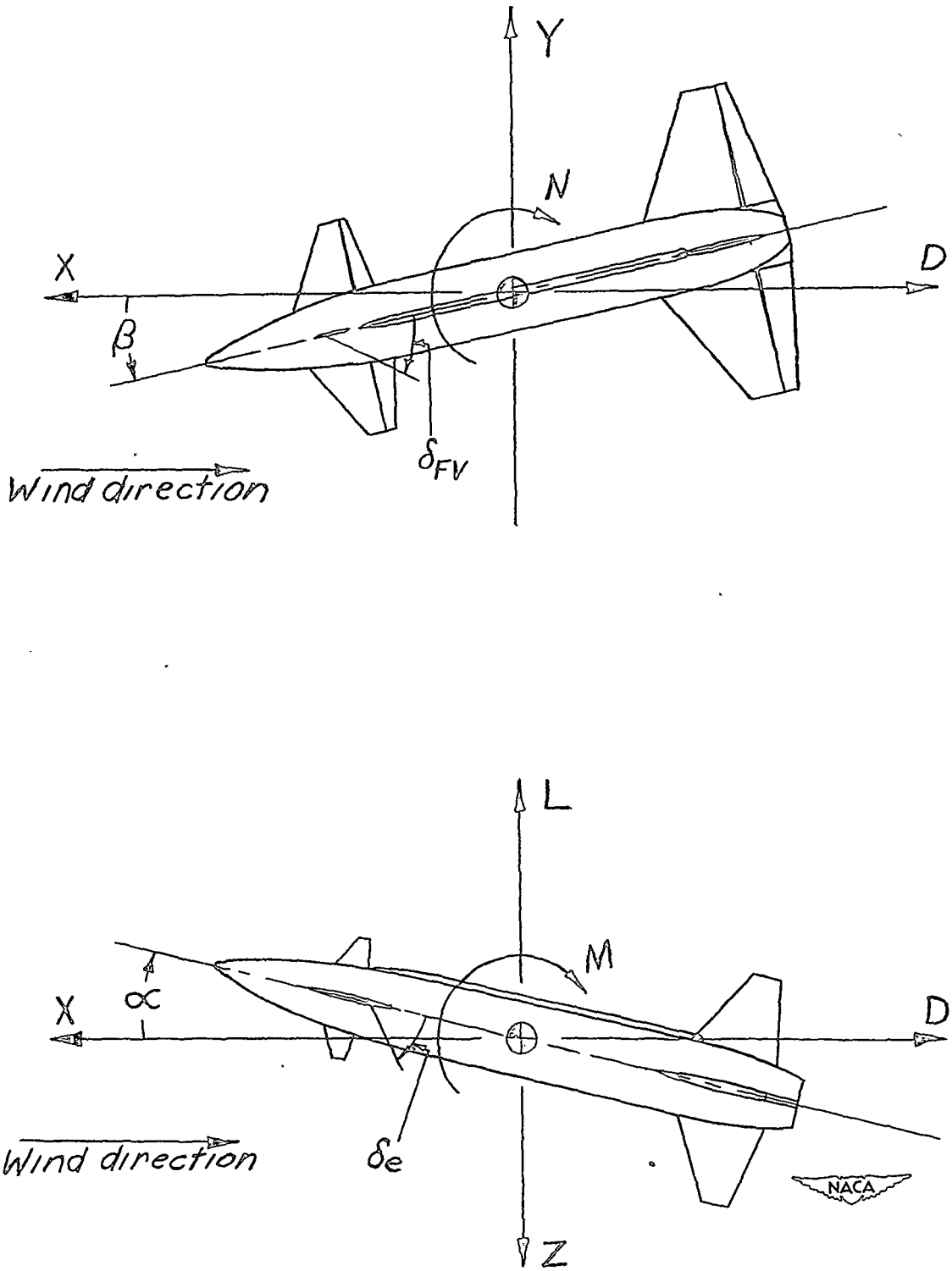

Figure 1.- System of wind axes. Arrows indicate positive directions of forces, moments, and angles.

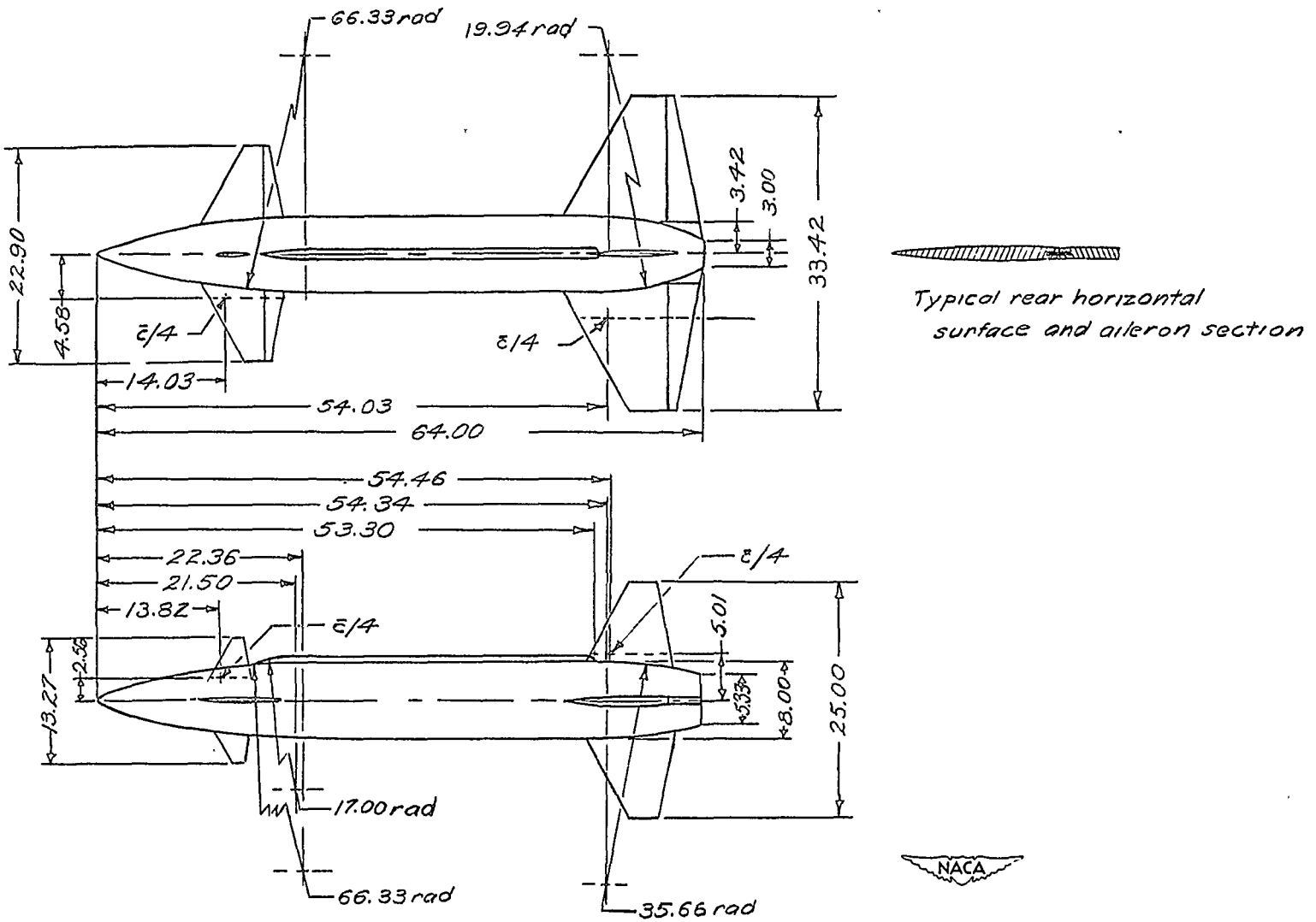

Figure 2.- General arrangment of $\frac{1}{6}$-scale Bell MX-776 used in the present investigation. All dimensions are in inches.

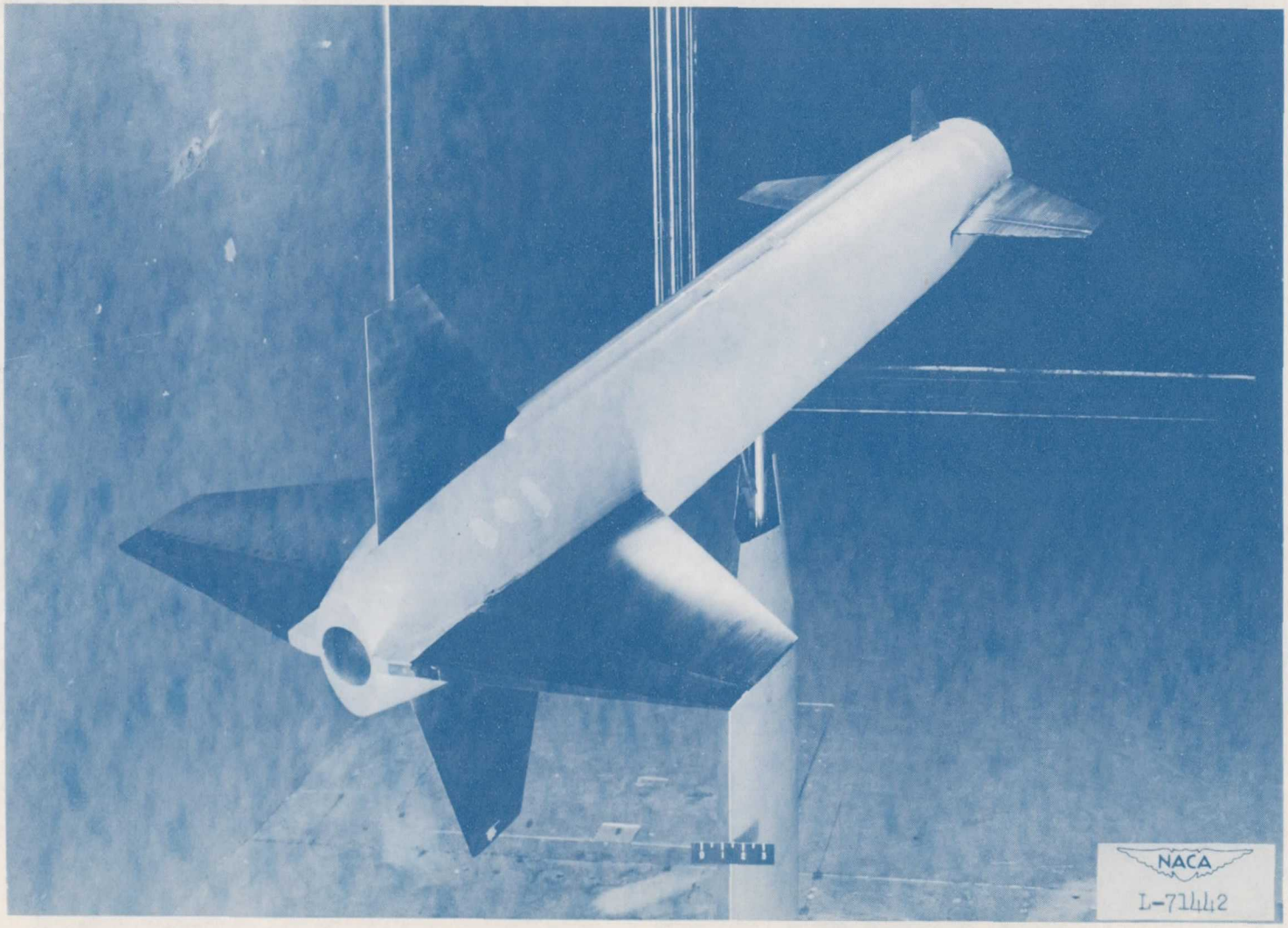

Figure 3.- Model mounted in Langley stability tunnel.

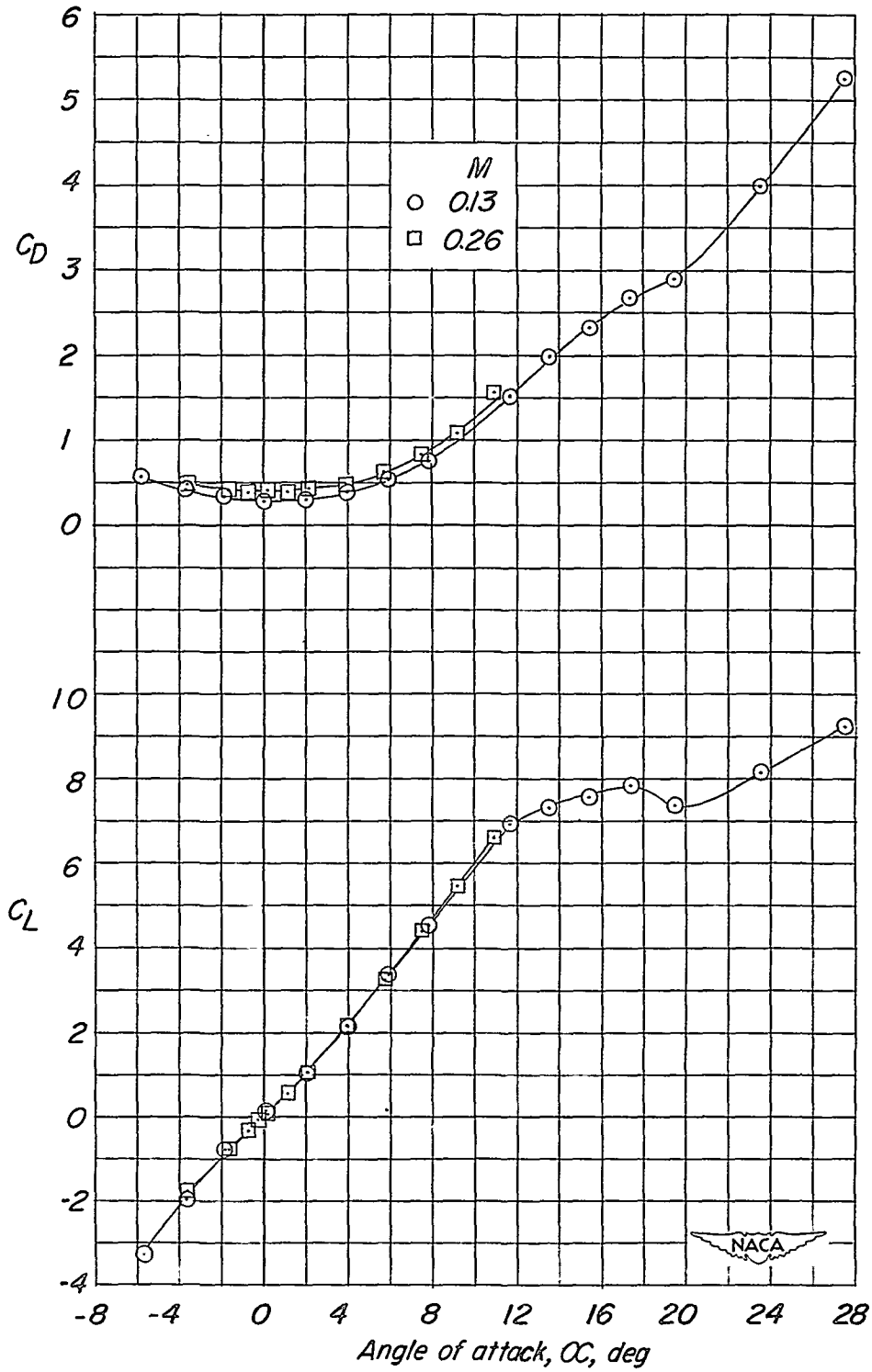

Figure 4.- Variation of lift, drag, and pitching-moment coefficients with angle of attack for Mach numbers of 0.13 and 0.26. Complete model; $\beta = 0$.

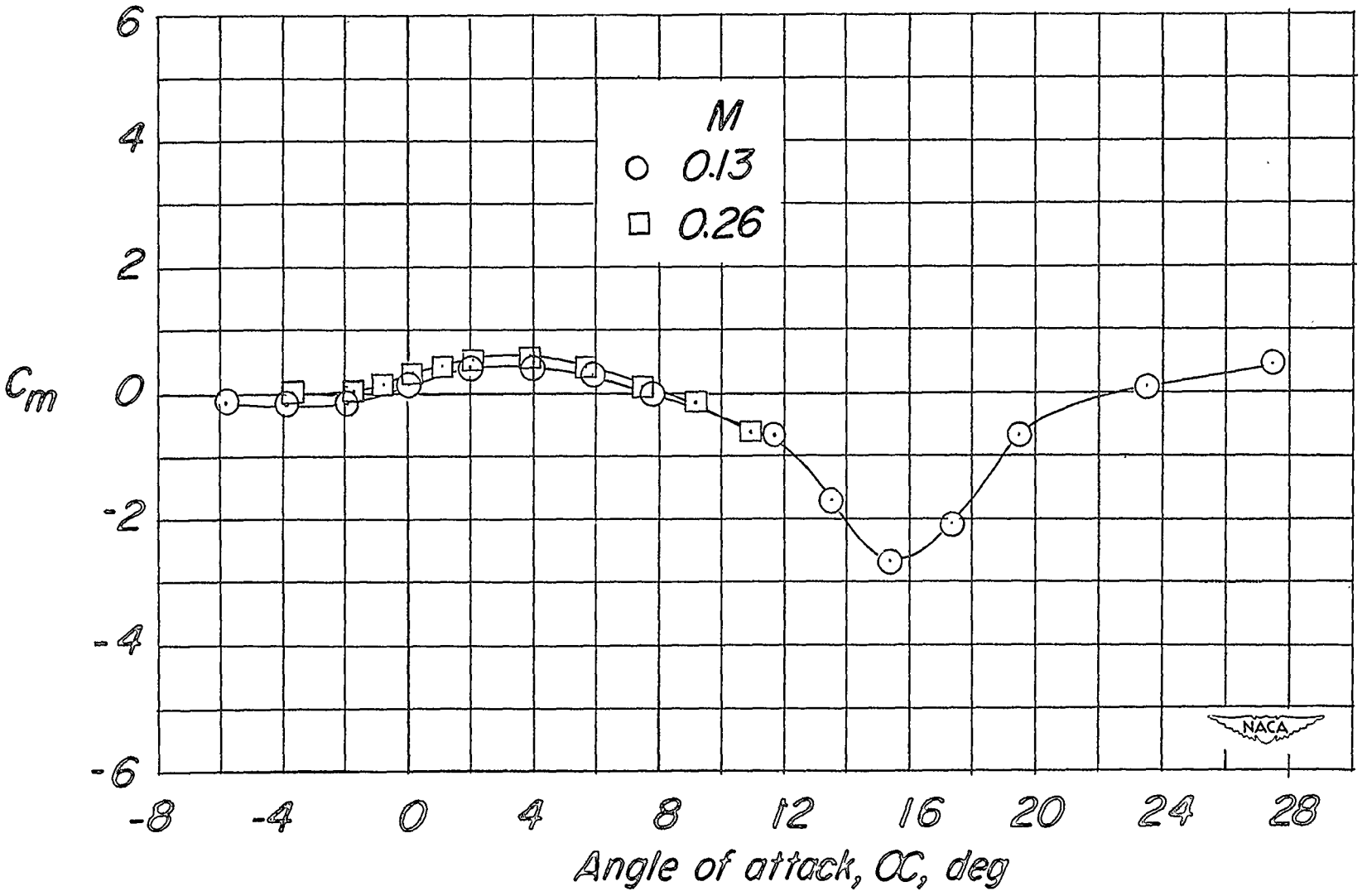

Figure 4.- Concluded.

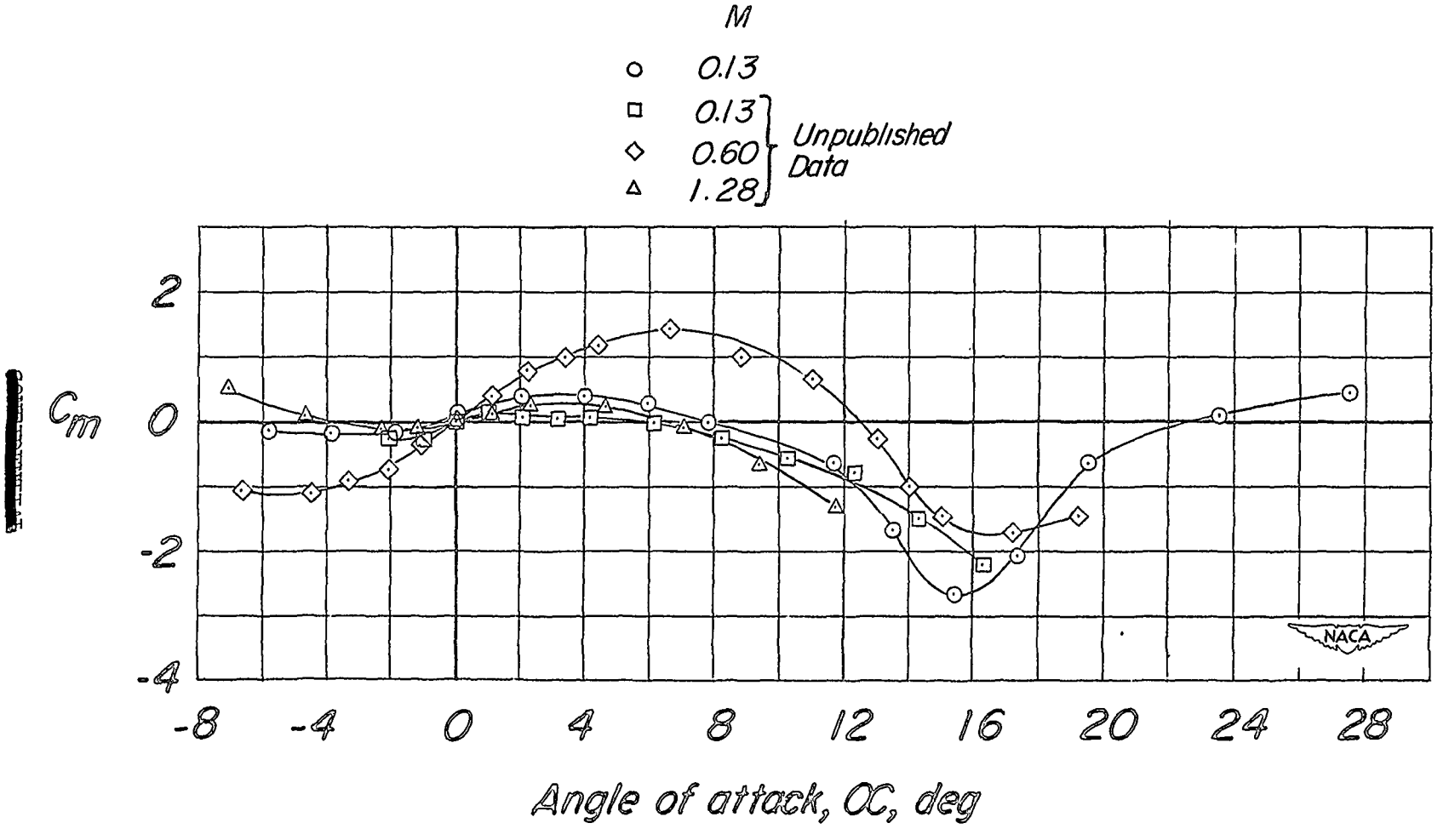

Figure 5.- Effect of Mach number on the variation of pitching-moment coefficients with angle of attack. Complete model; $\beta = 0$.

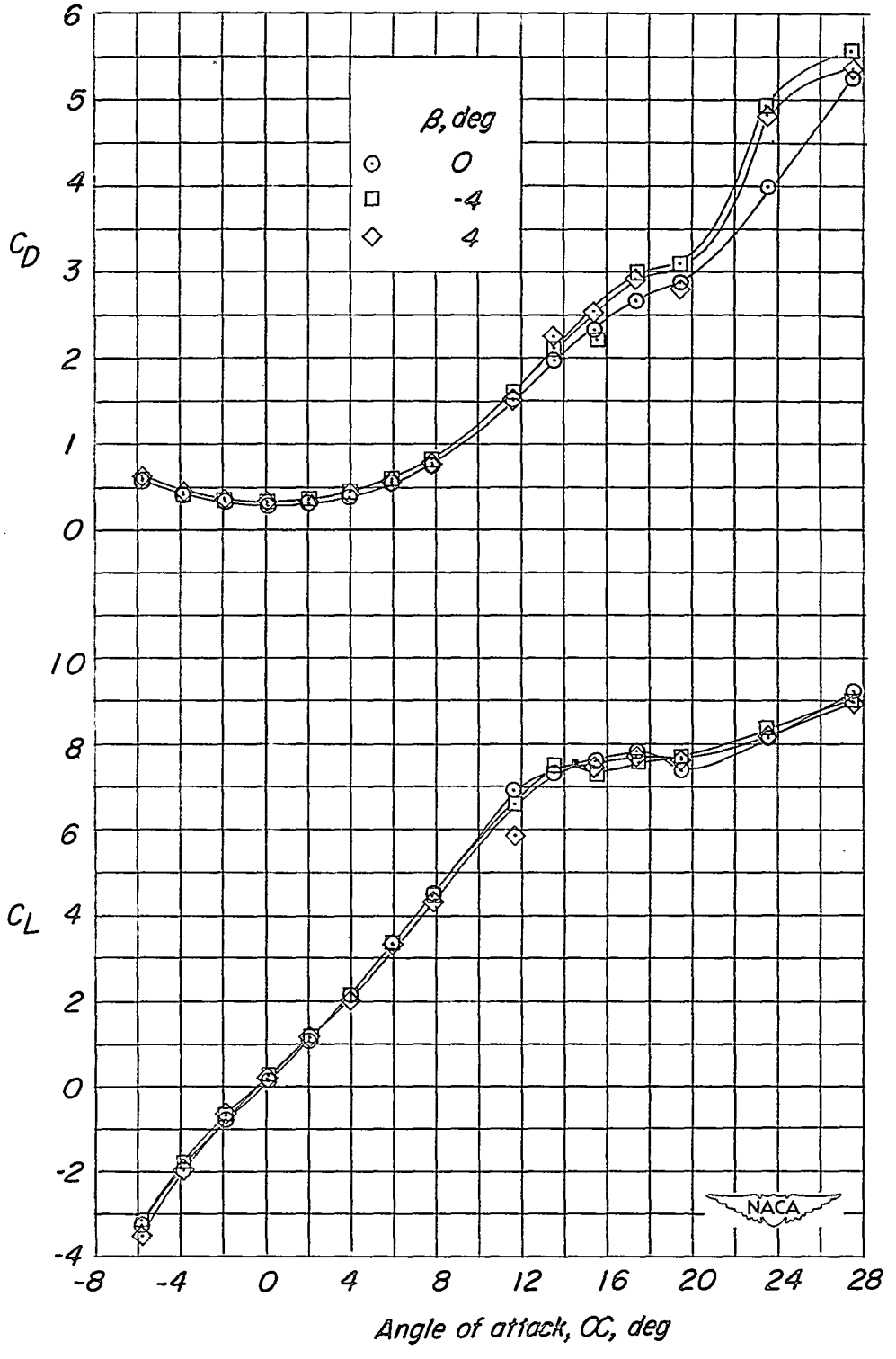

Figure 6.- Effect of small sideslip angles on the variation of lift, drag, and pitching-moment coefficients with angle of attack. Complete model.

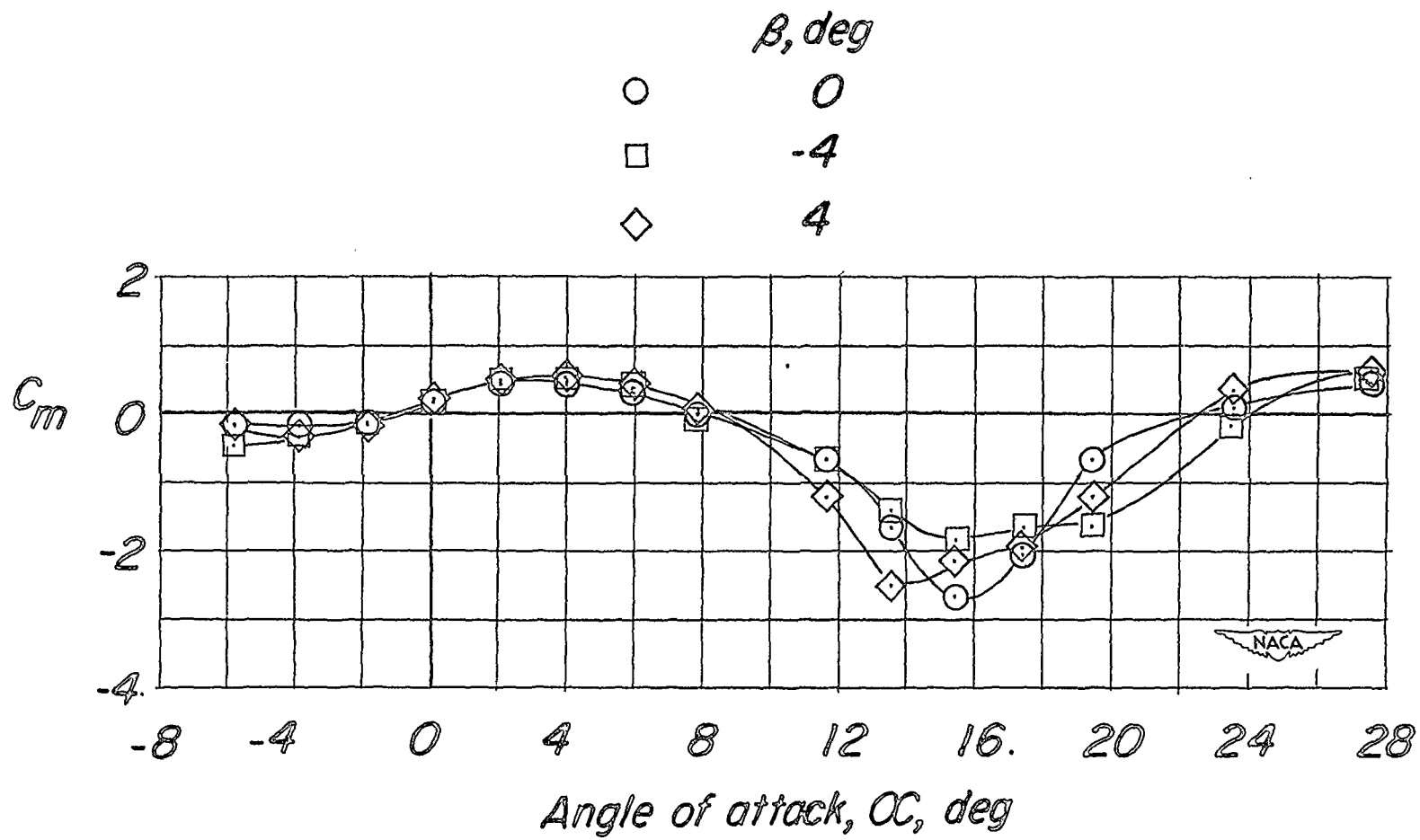

Figure 6.- Concluded.

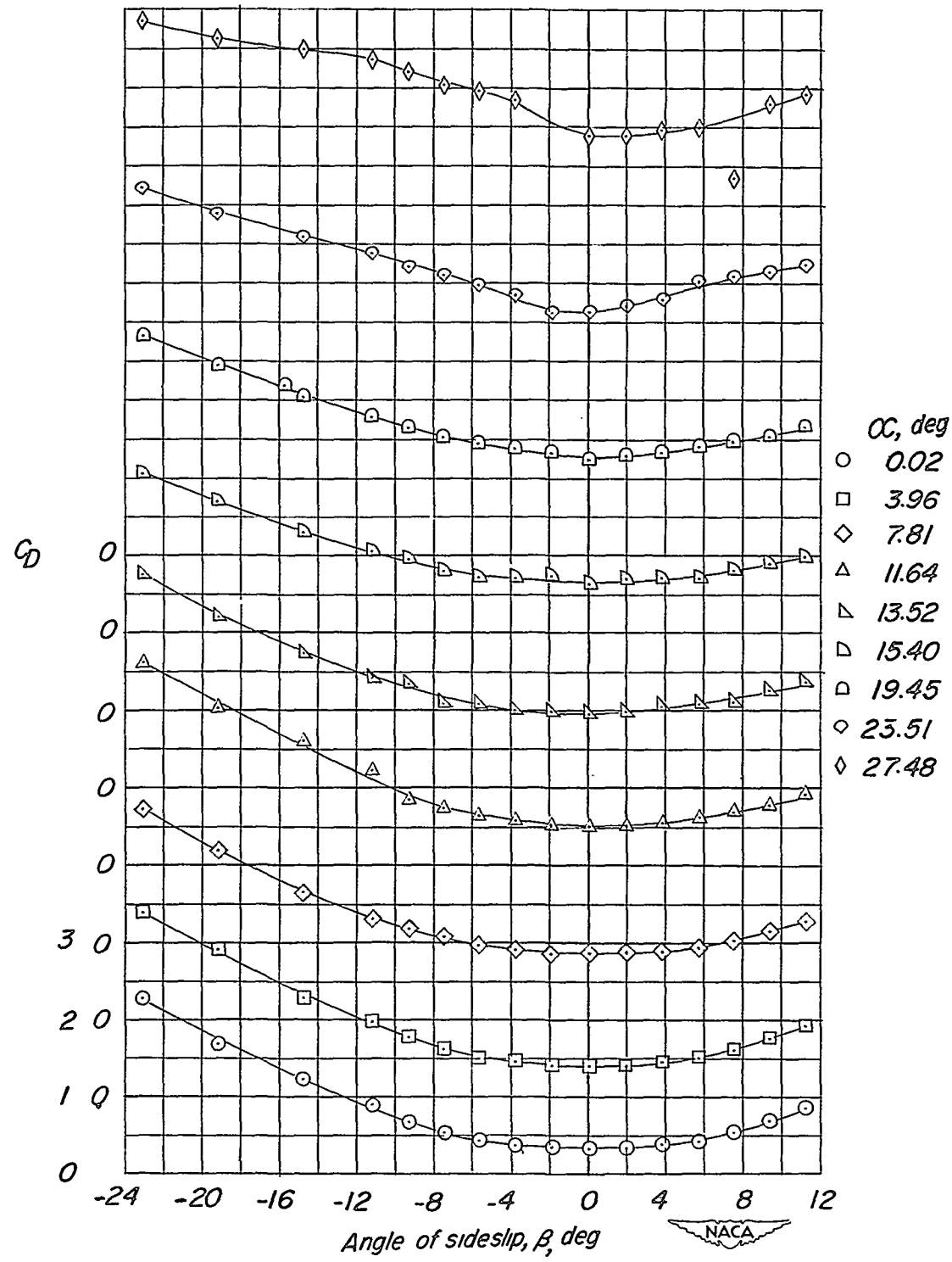

Figure 7.- Variation of lift, drag, and pitching moments with sideslip angle for various angles of attack. Complete model.

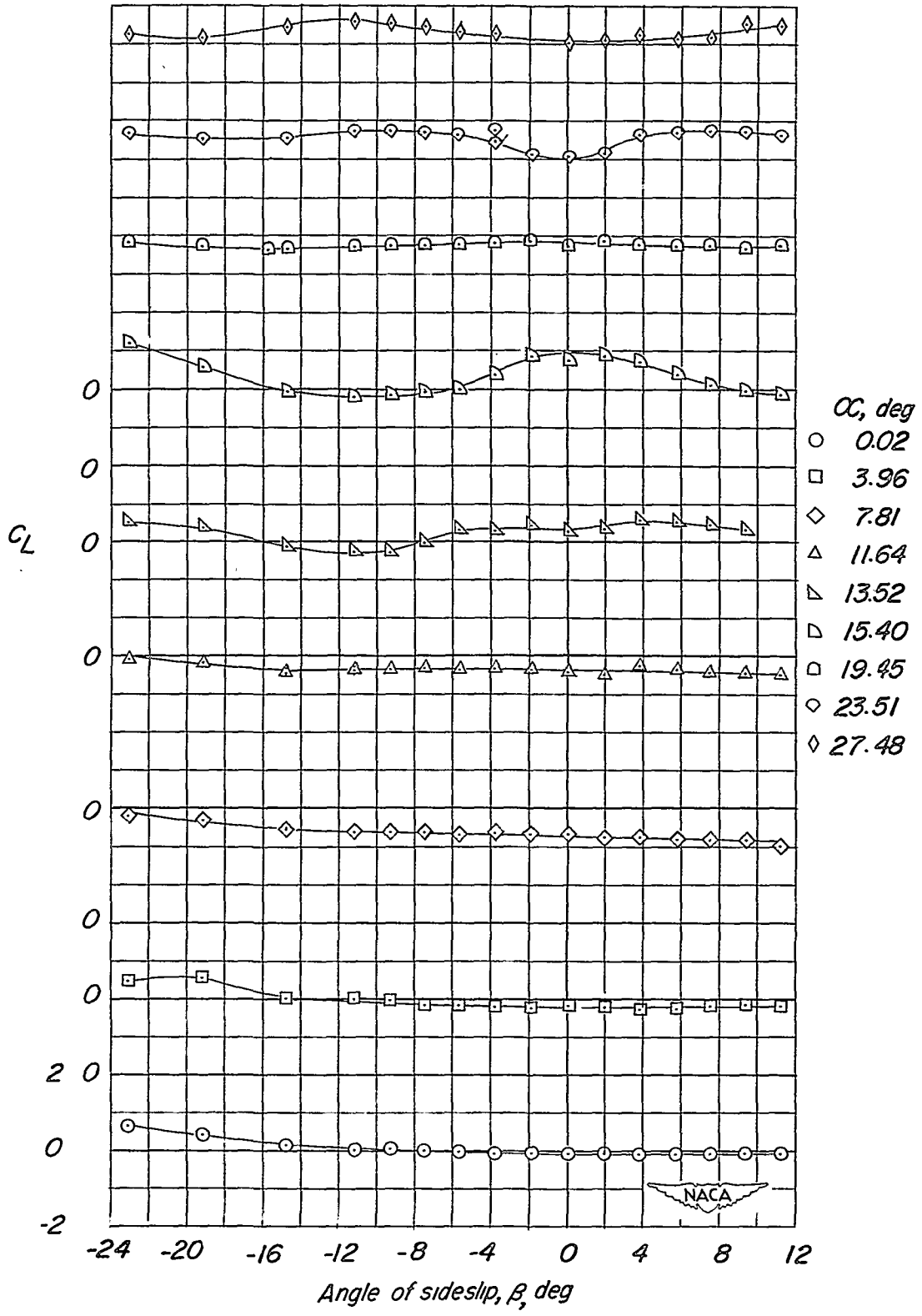

Figure 7.- Continued.

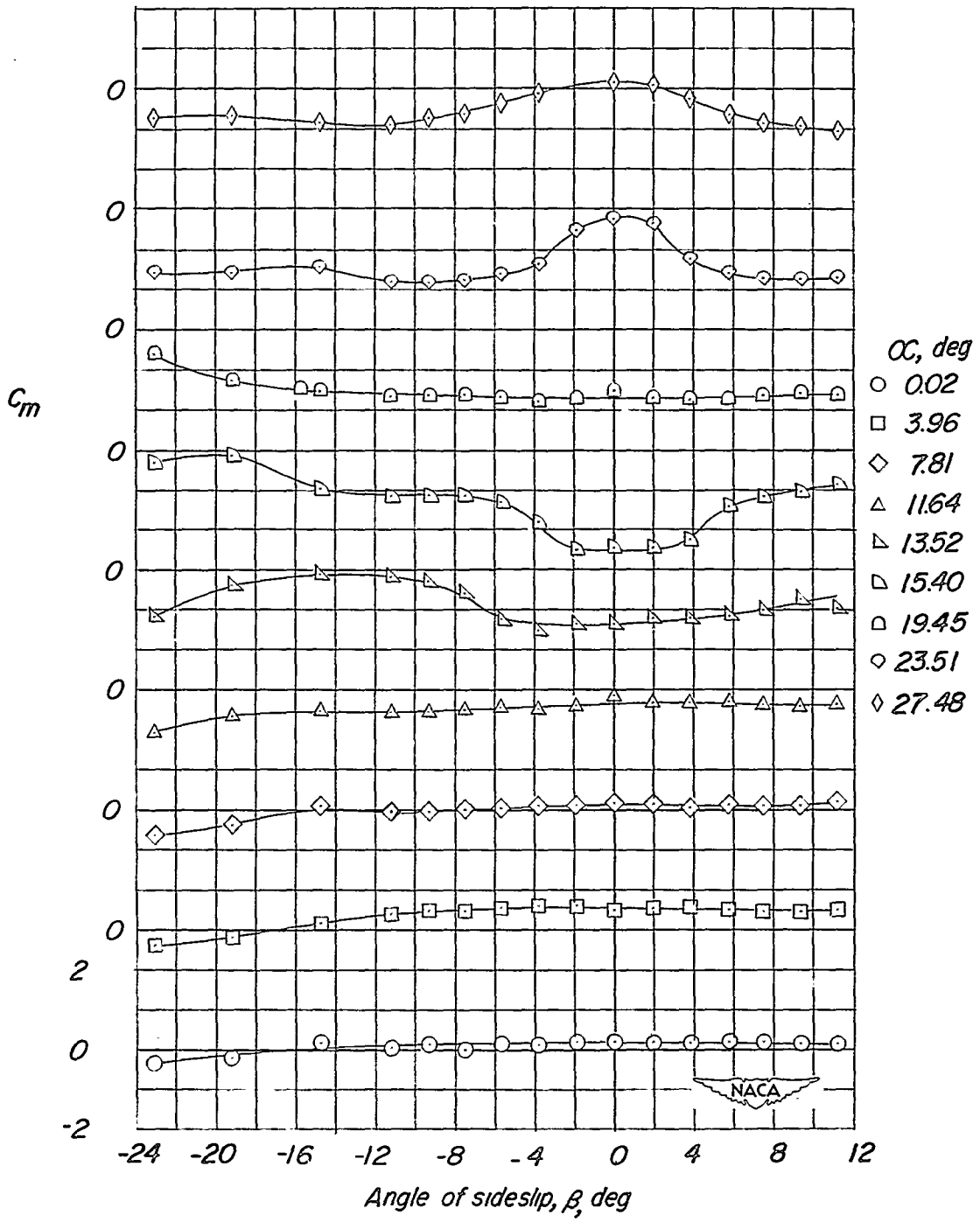

Figure 7.- Concluded.

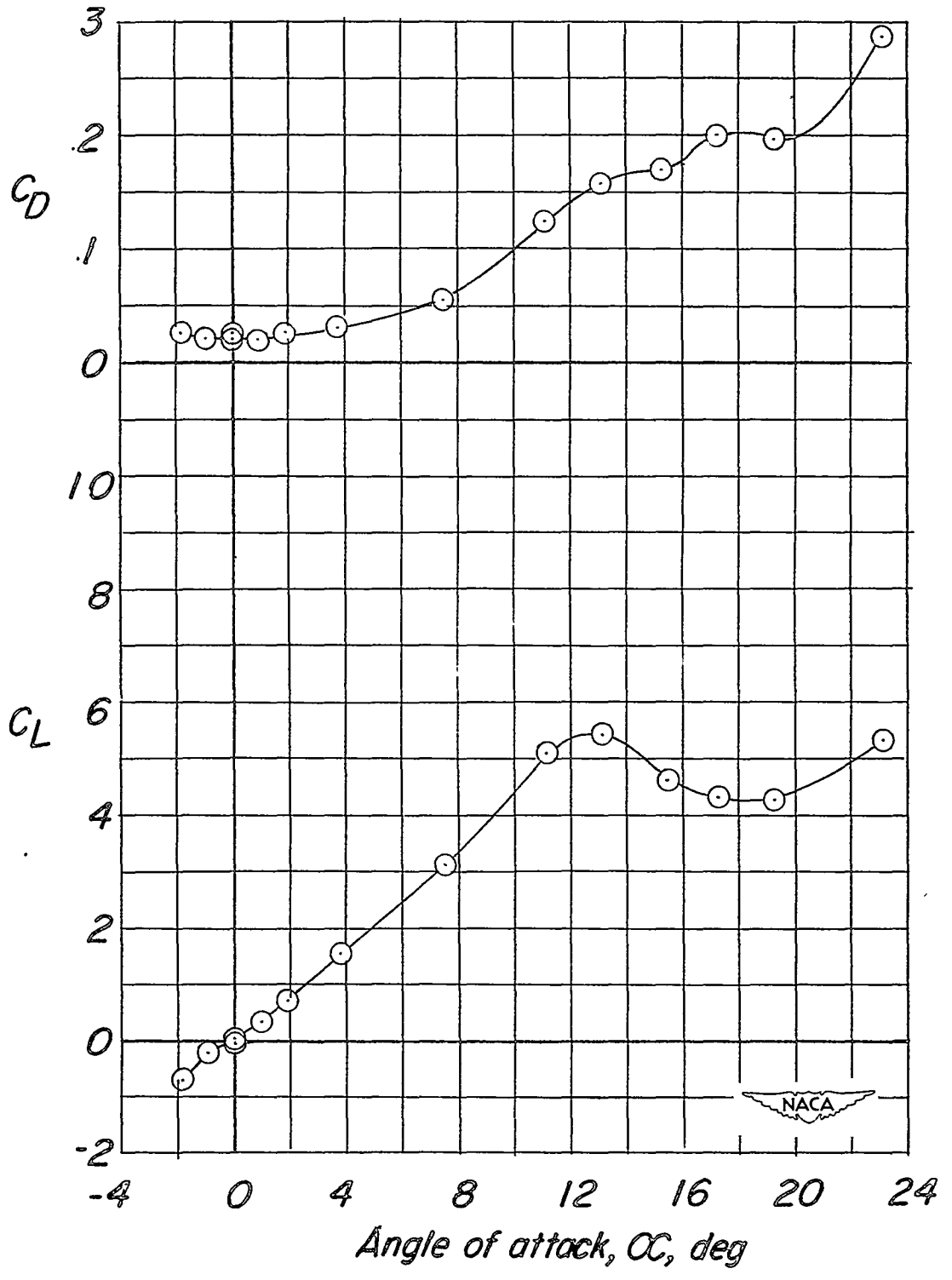

Figure 8.- Variation of lift, drag, and pitching-moment coefficients with angle of attack for the model with forward horizontal surfaces removed. $\beta = 0$.

[redacted]

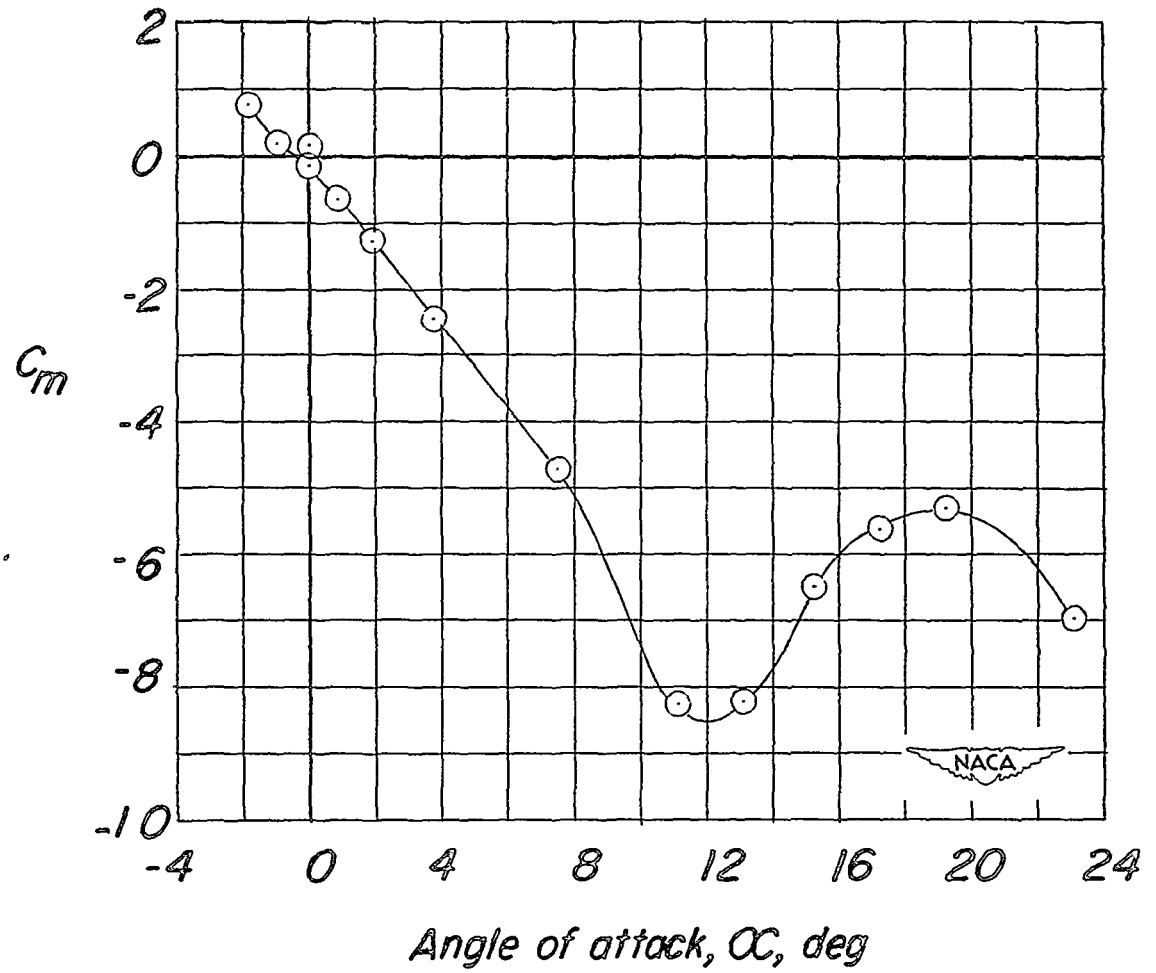

Figure 8.- Concluded.

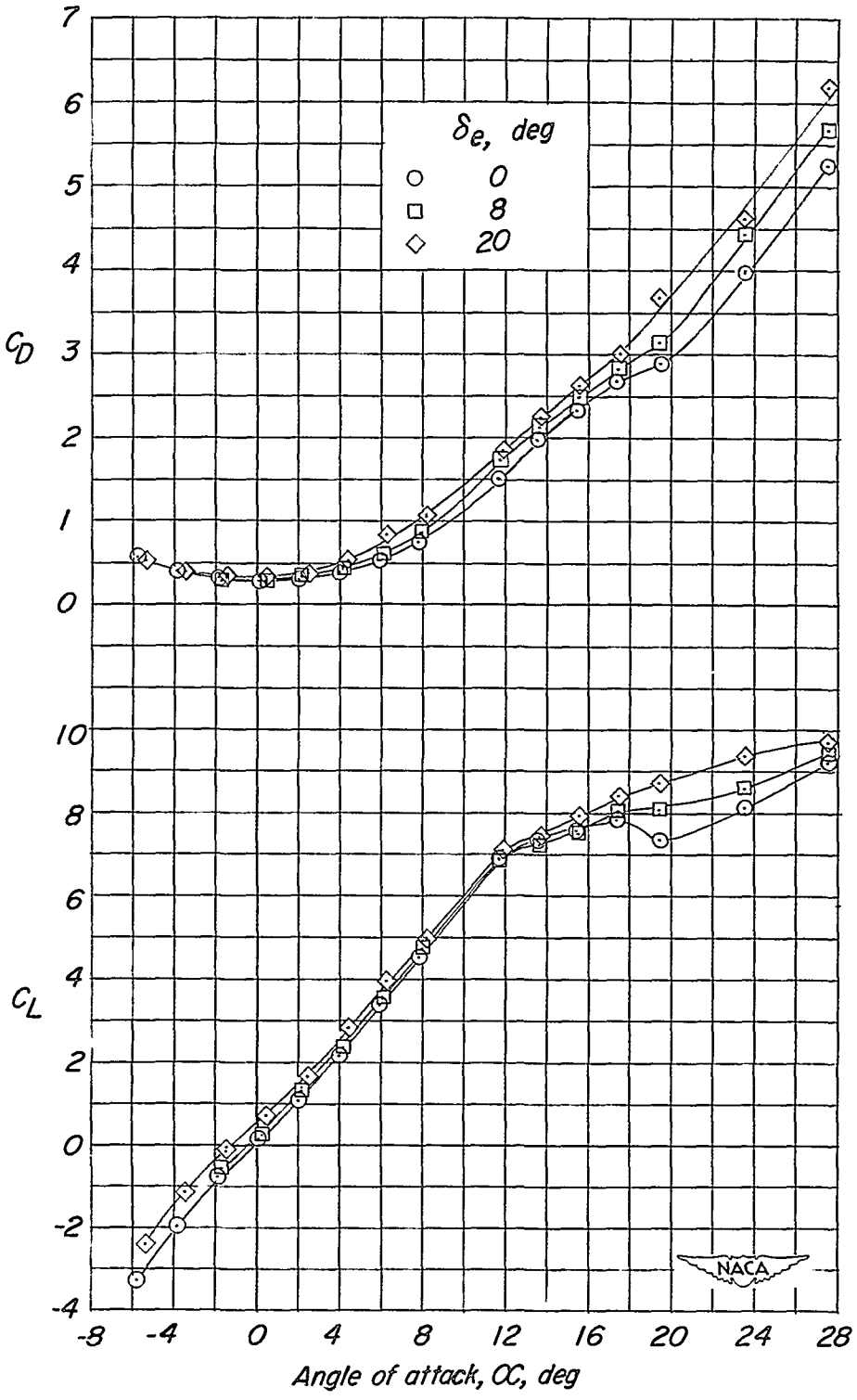

Figure 9.- Variation of lift, drag, and pitching-moment coefficients with angle of attack for model with elevators deflected 0°, 8°, and 20°. Complete model; $\beta = 0$.

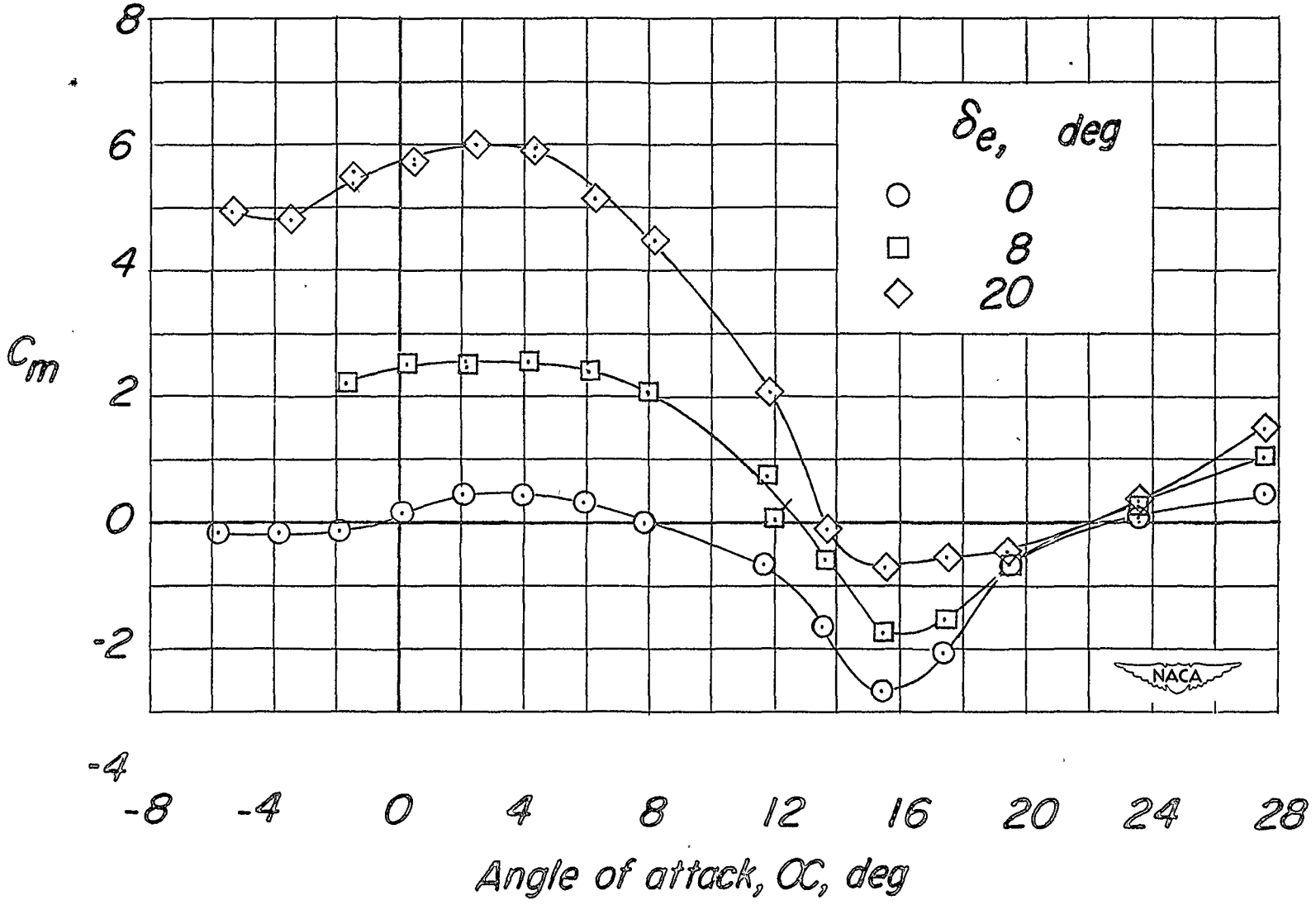

Figure 9.- Concluded.

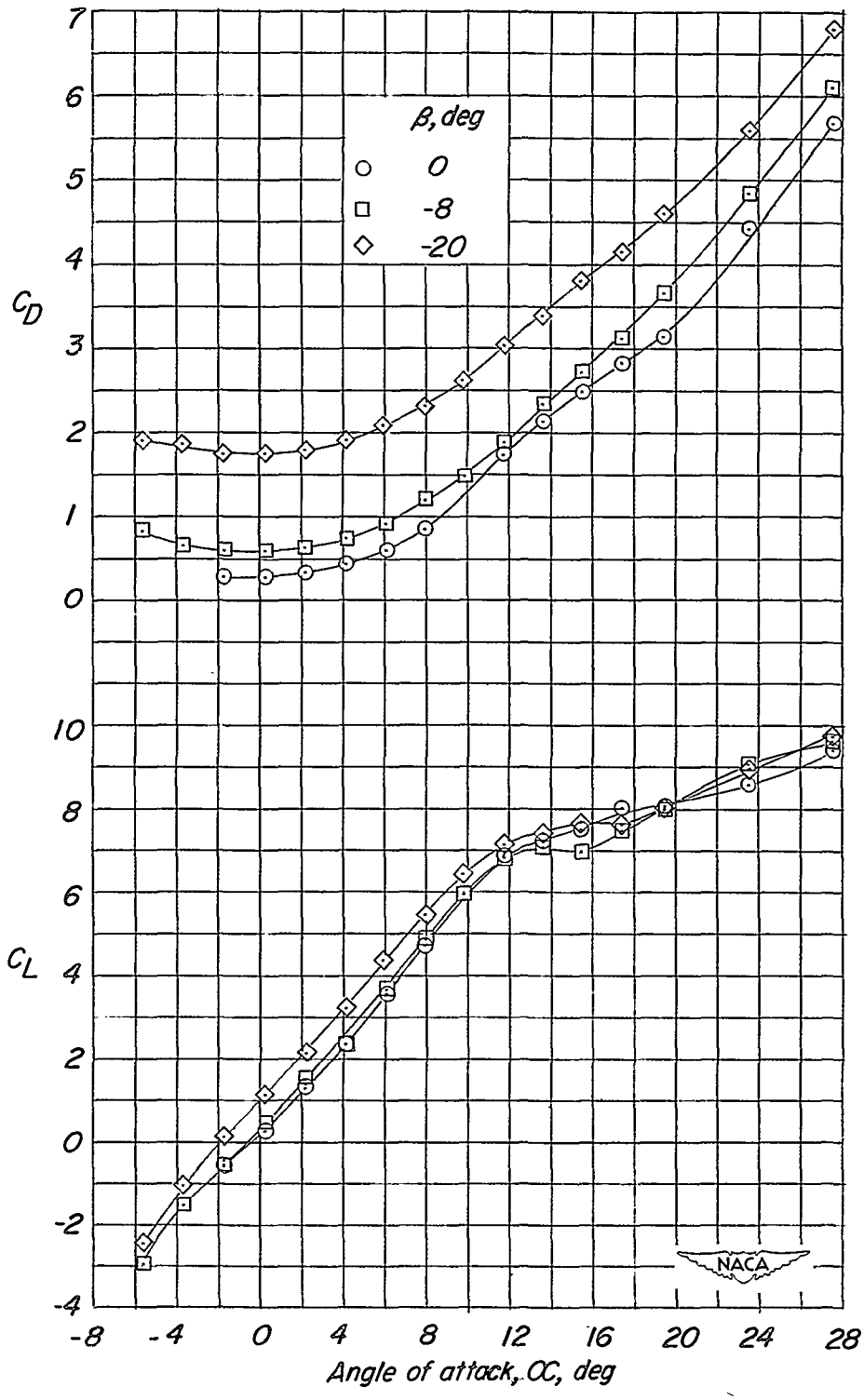

Figure 10.- Effect of sideslip angle on the variation of lift, drag, and pitching-moment coefficients with angle of attack for the model with elevator deflected 8°. Complete model.

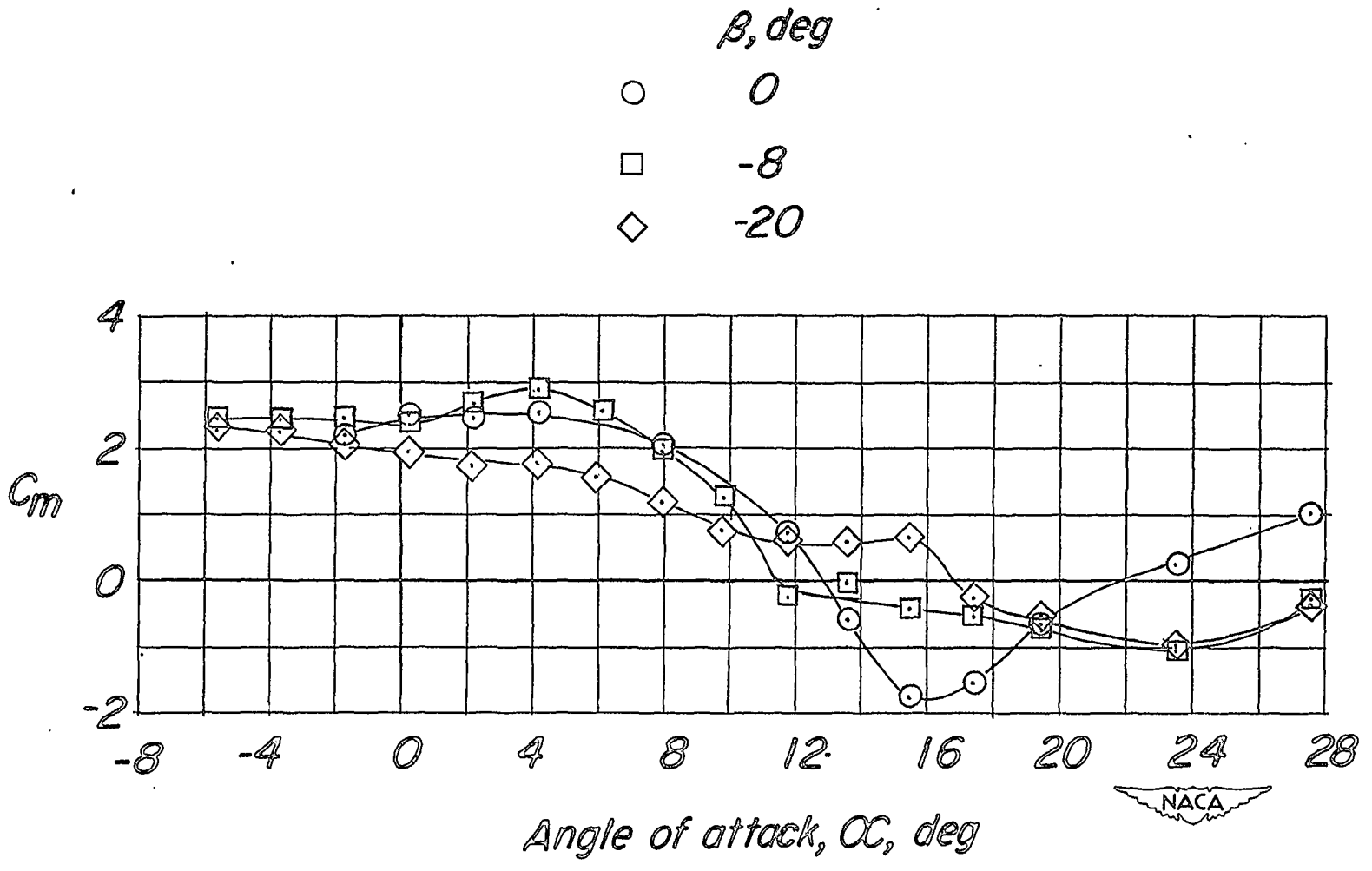

Figure 10.- Concluded.

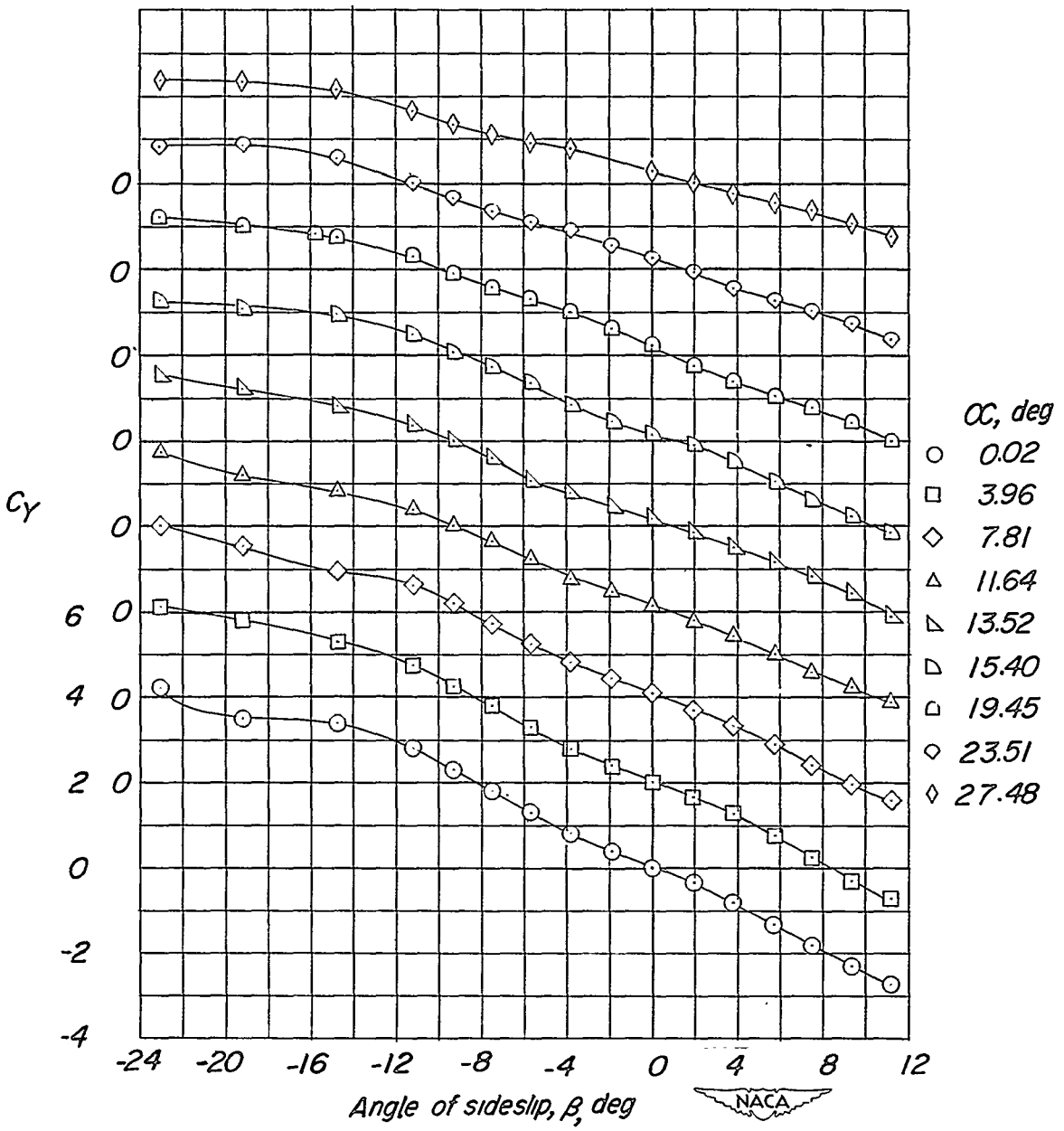

Figure 11.- Variation of side-force, yawing-moment, and rolling-moment coefficients with sideslip angle. Complete model.

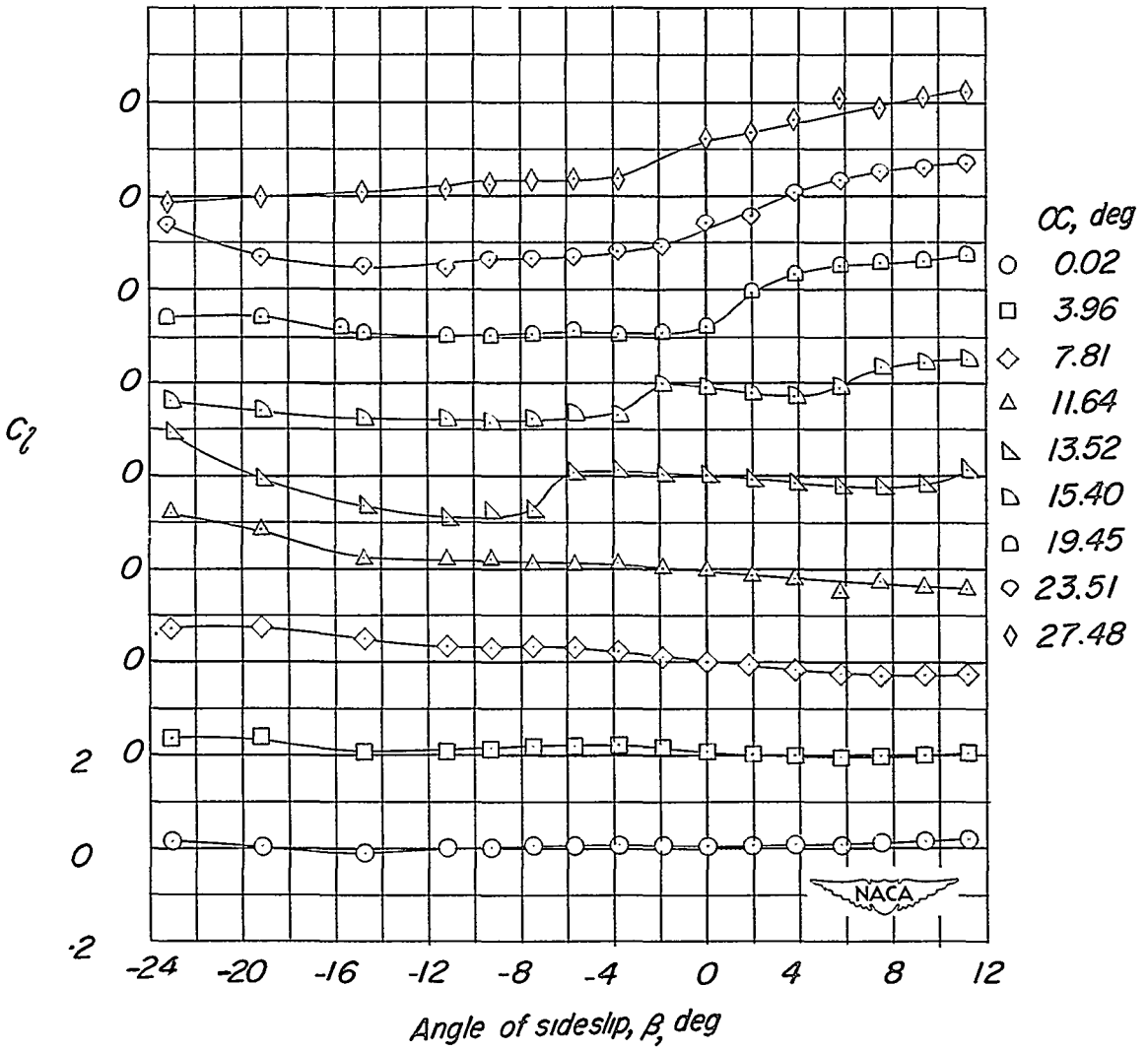

Figure 11.- Continued.

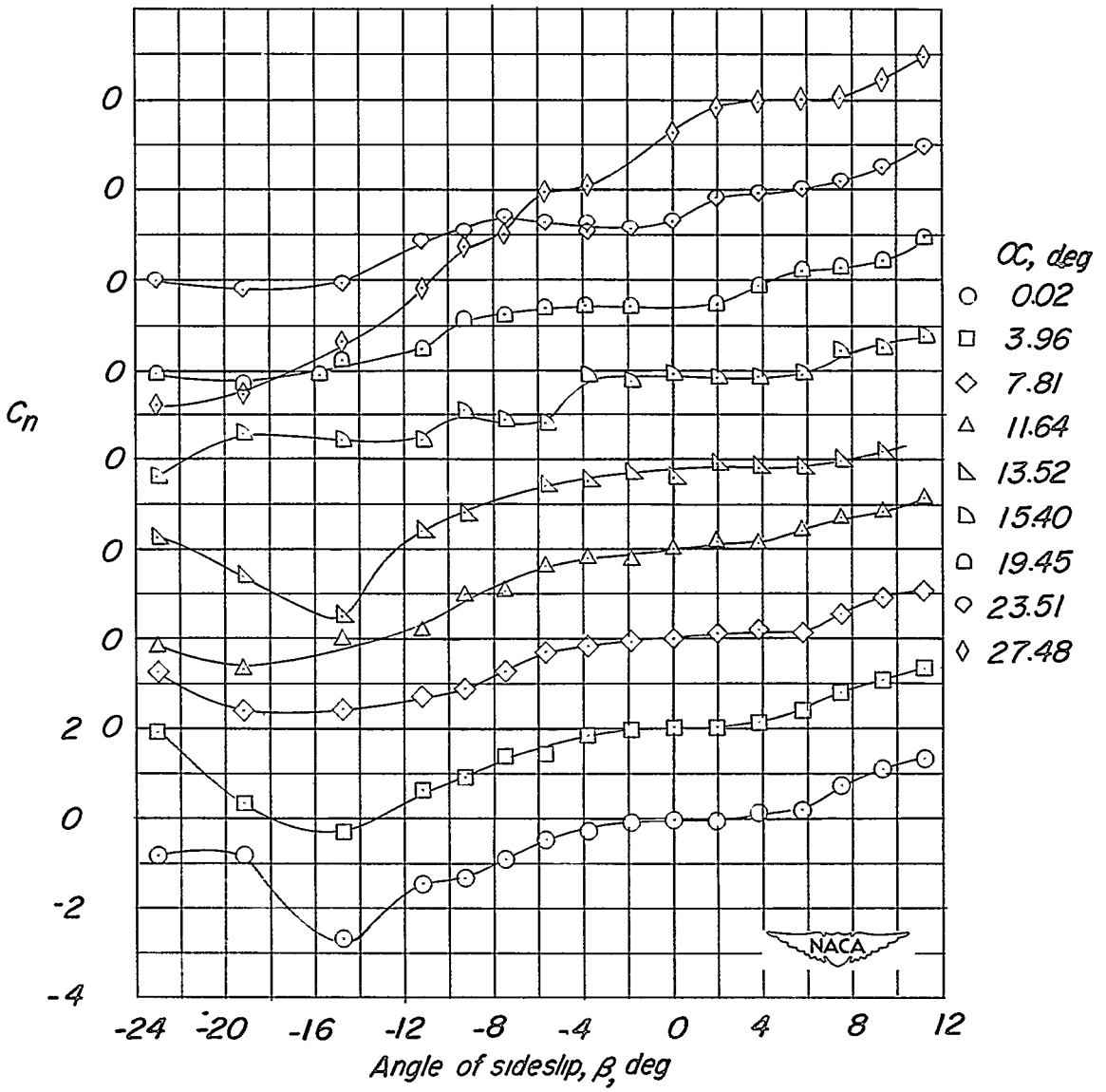

Figure 11.- Concluded.

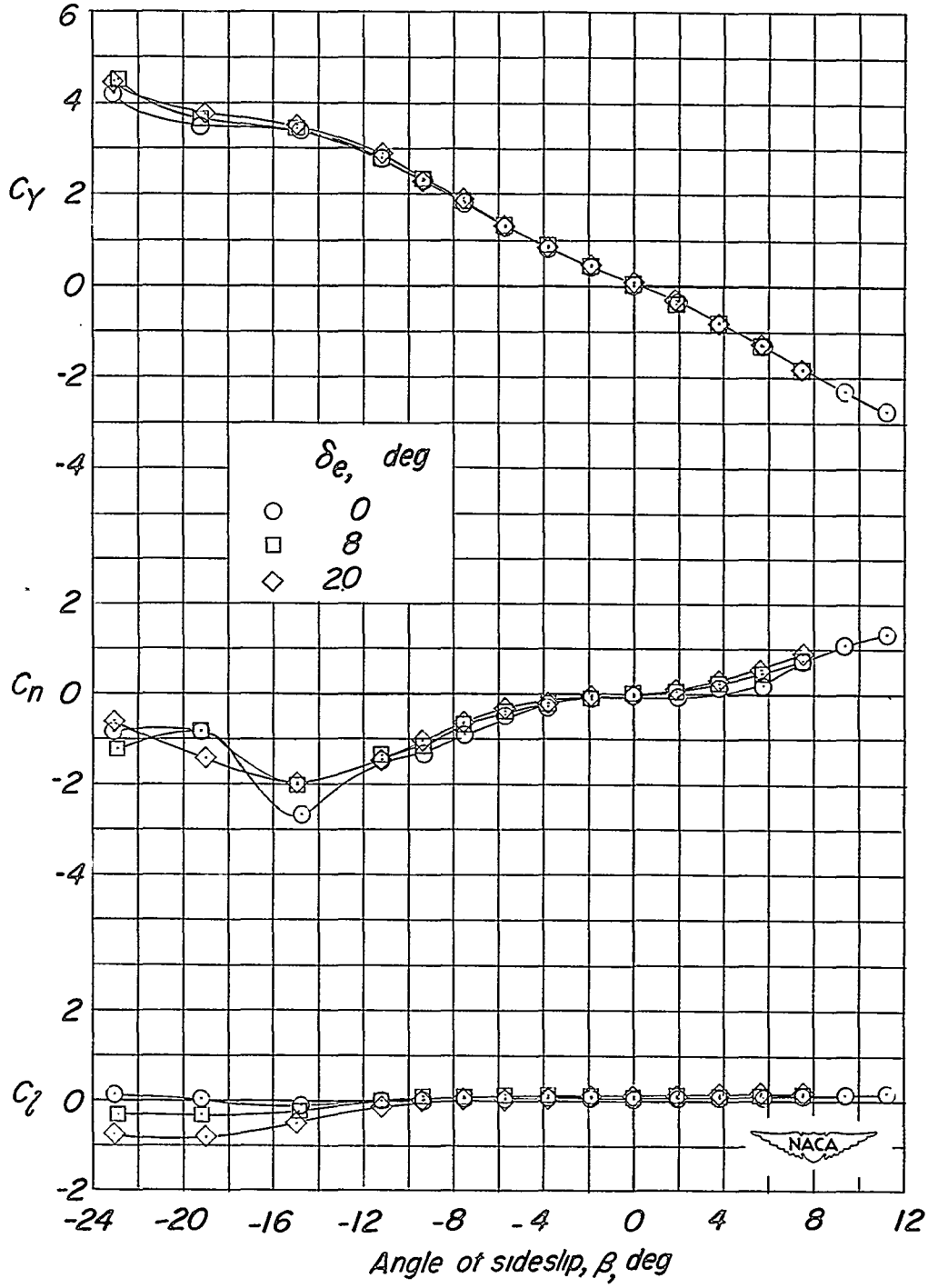

(a) $\alpha = 0^\circ$.

Figure 12.- Variation of side-force, yawing-moment, and rolling-moment coefficients with sideslip angle for model with elevators deflected 0°, 8°, and 20°. Complete model.

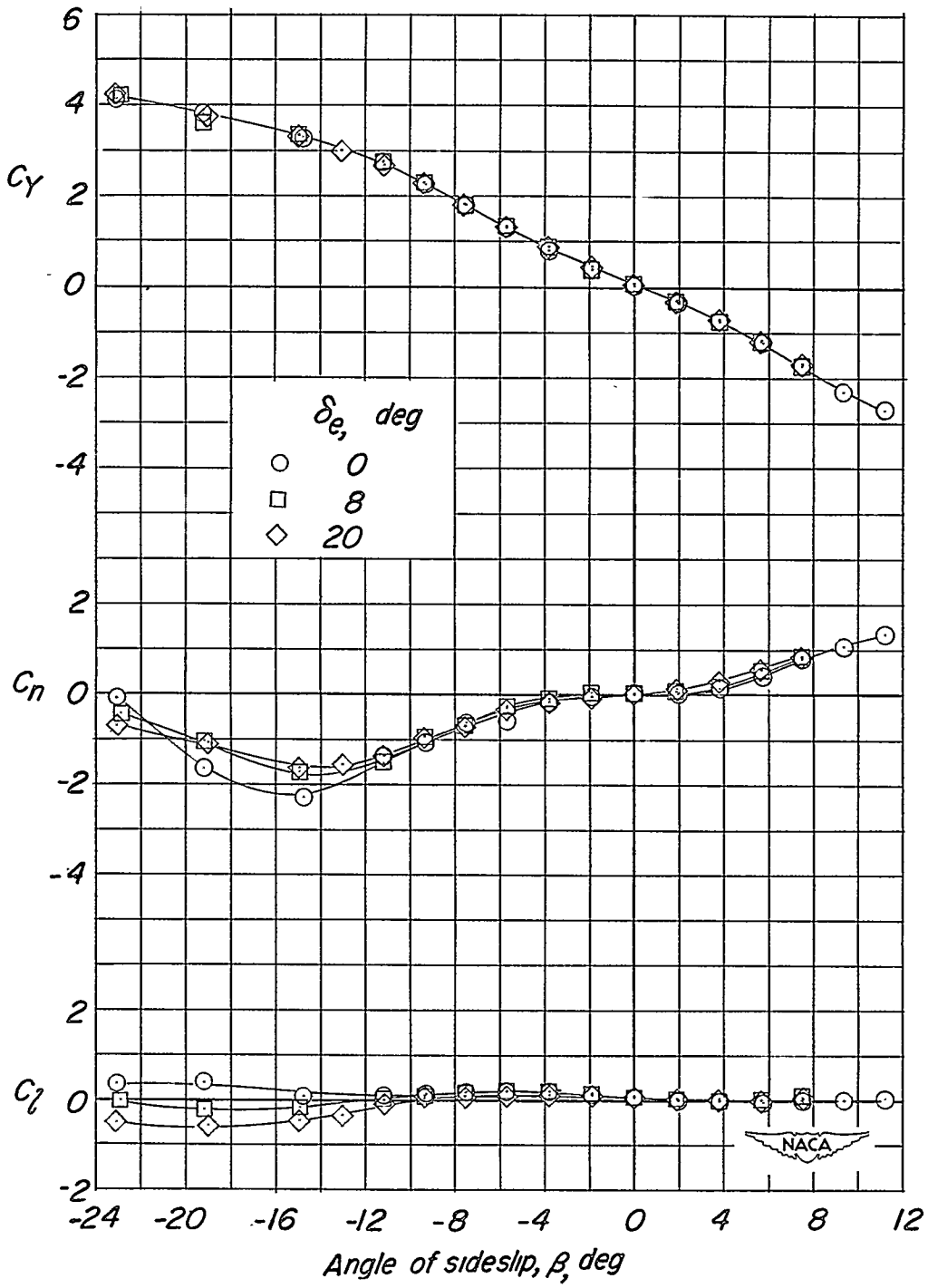

(b) $\alpha = 4^\circ$.

Figure 12.- Continued.

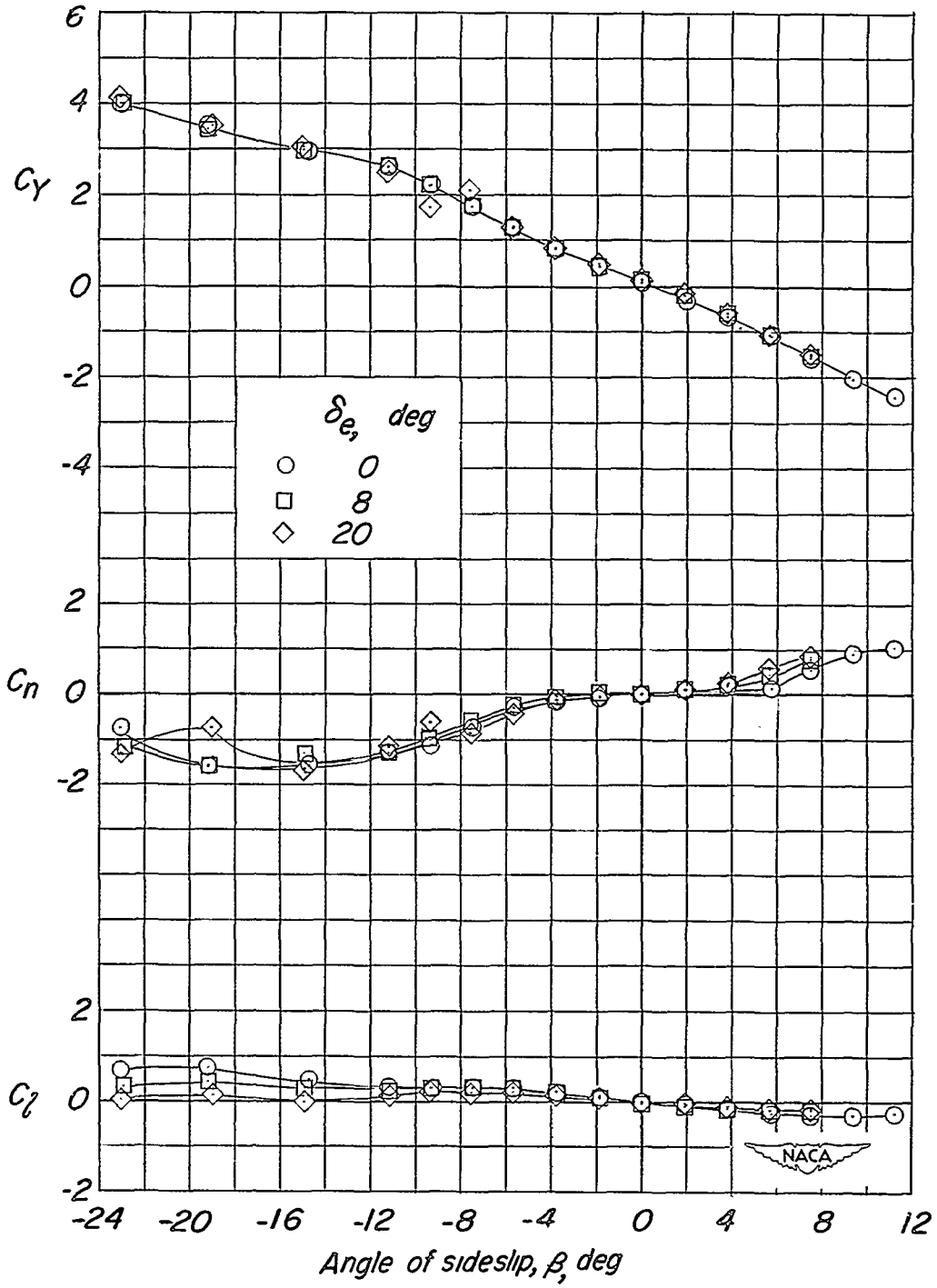

(c) $\alpha = 8^\circ$.

Figure 12.- Continued.

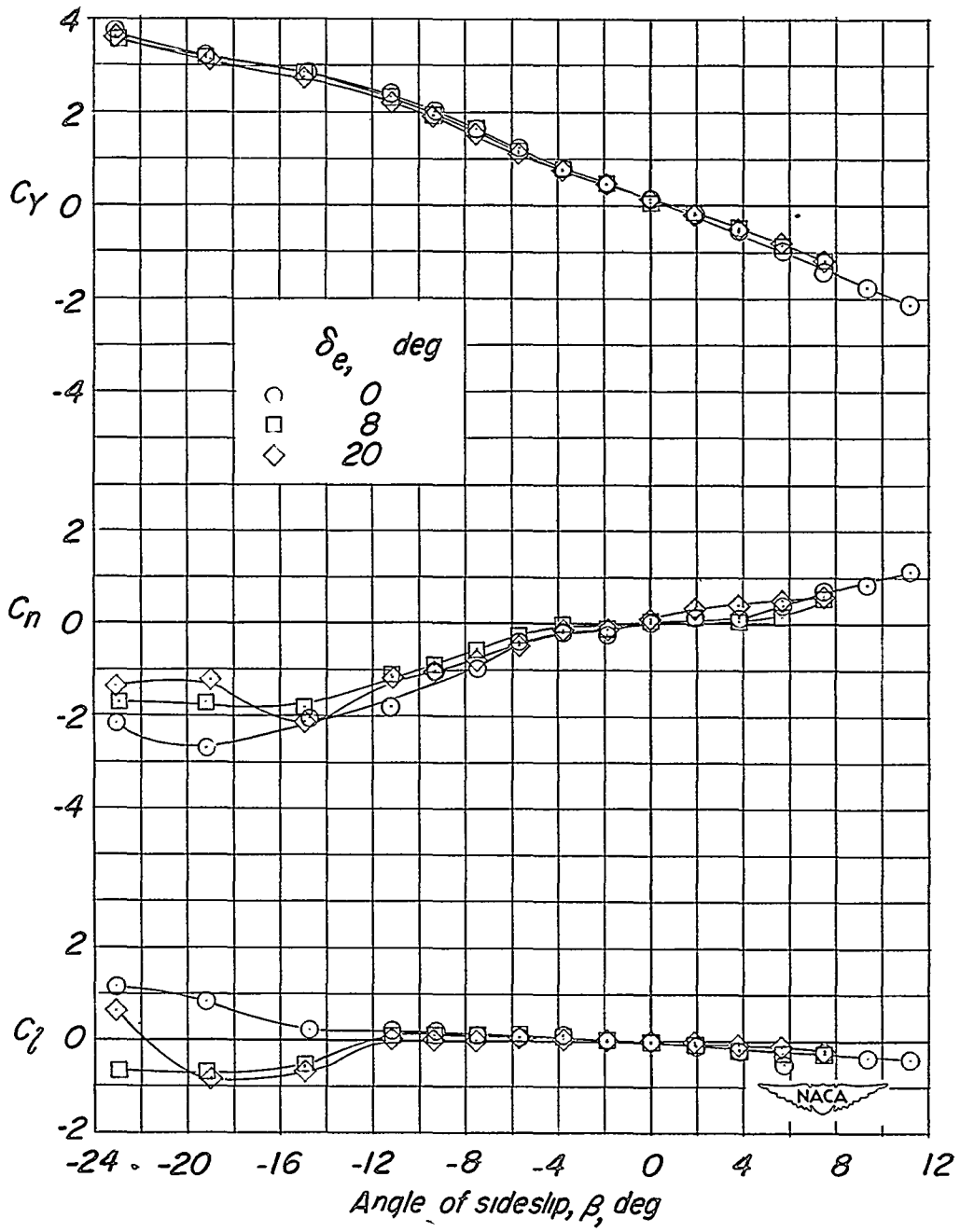

(d) $\alpha = 12^\circ$

Figure 12.- Concluded.

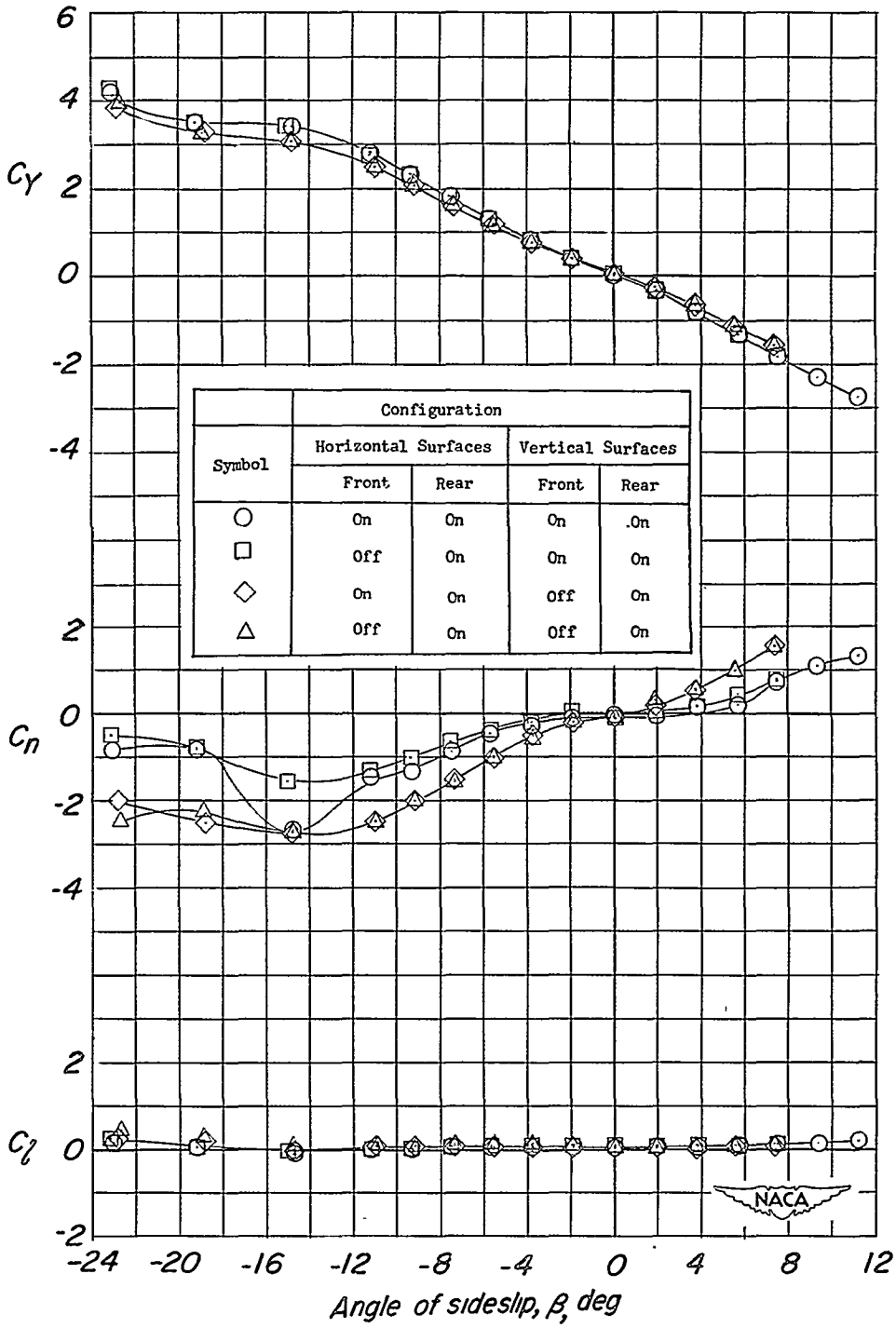

Symbol	Configuration			
	Horizontal Surfaces		Vertical Surfaces	
	Front	Rear	Front	Rear
○	On	On	On	On
□	Off	On	On	On
◇	On	On	Off	On
△	Off	On	Off	On

(a) $\alpha = 0^{\circ}$.

Figure 13.- Variation of side-force, yawing-moment, and rolling-moment coefficients with sideslip angle for the model with various forward surfaces removed.

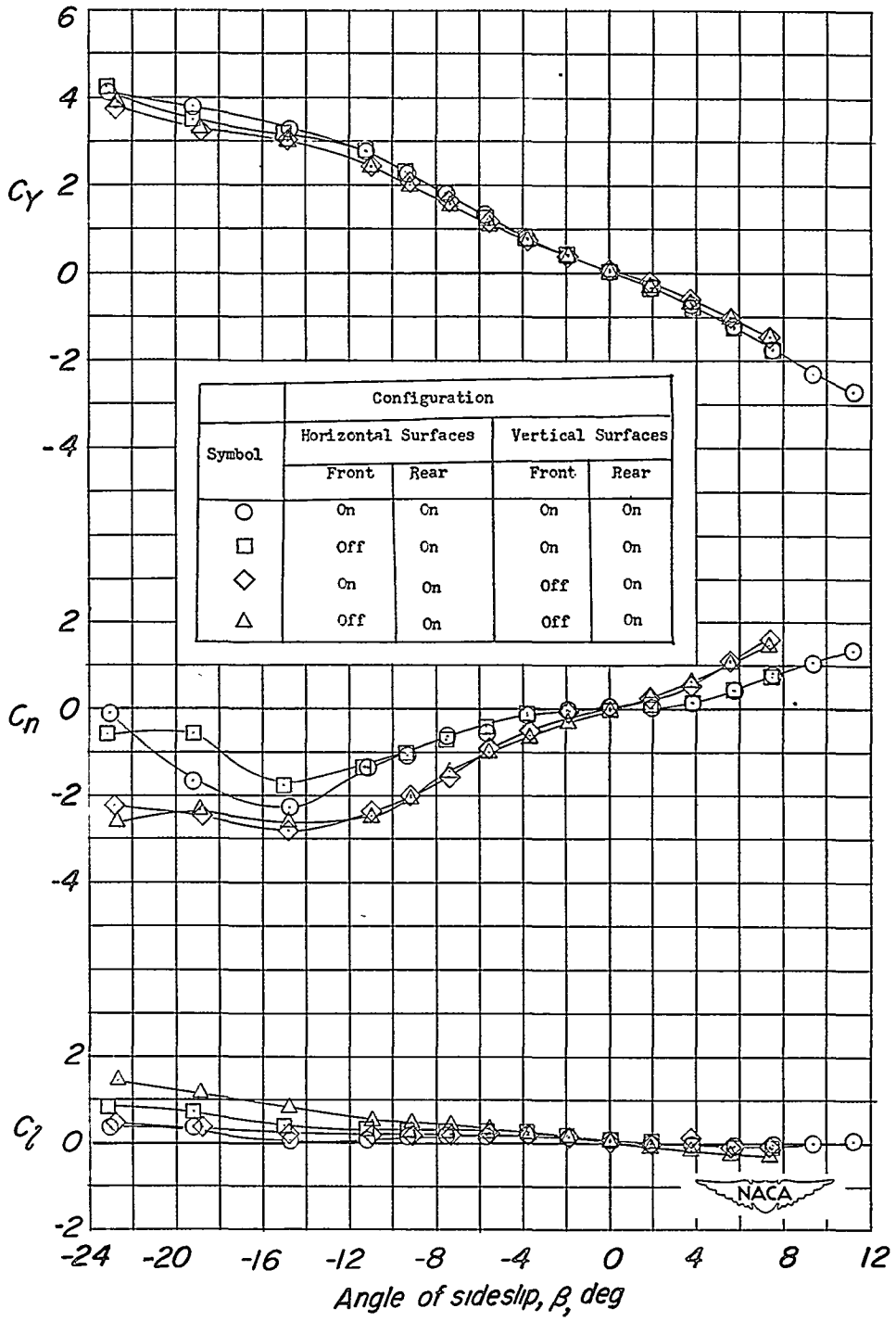

(b) $\alpha = 4^{\circ}$.

Figure 13.- Continued.

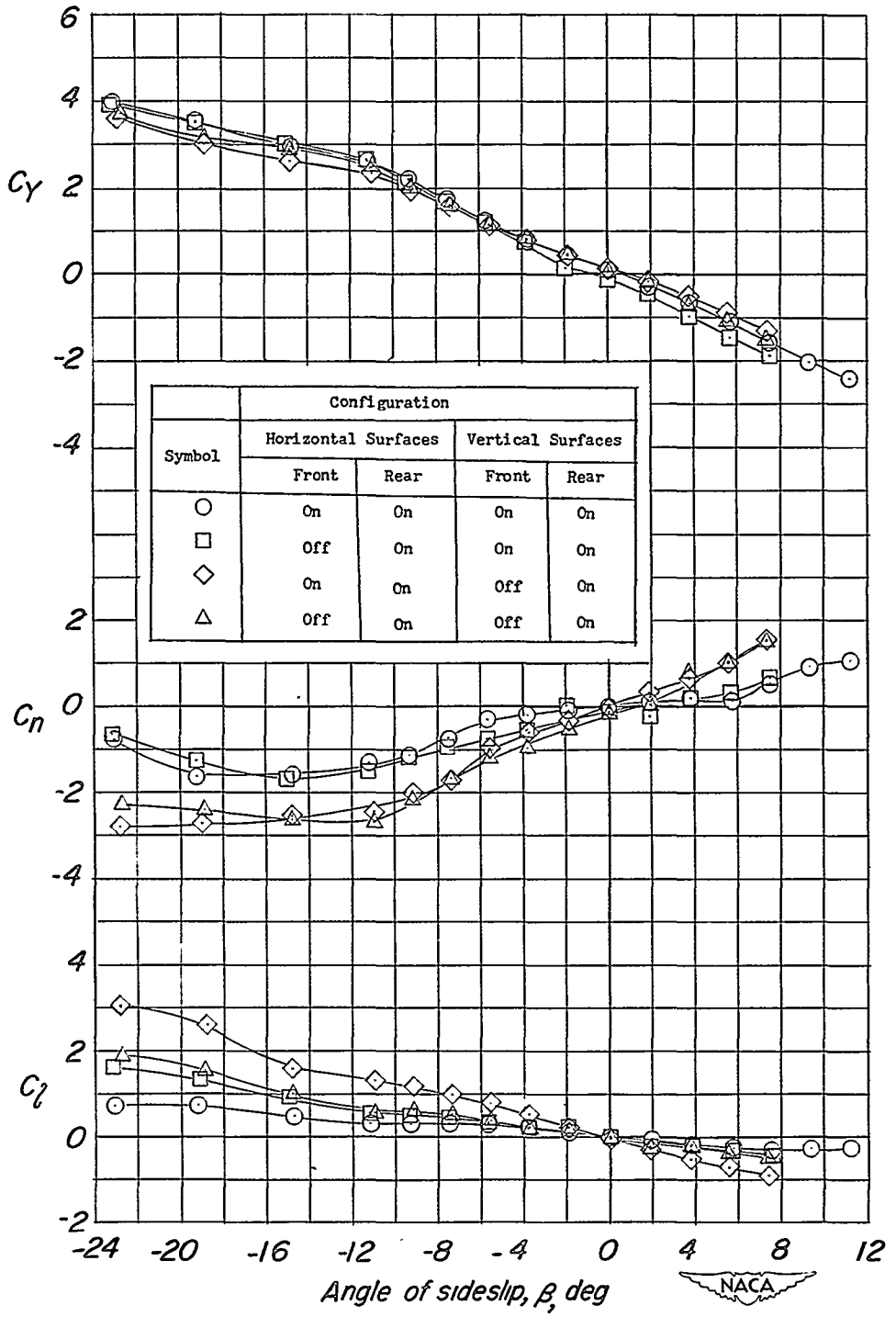

(c) $\alpha = 8^\circ$.

Figure 13.- Continued.

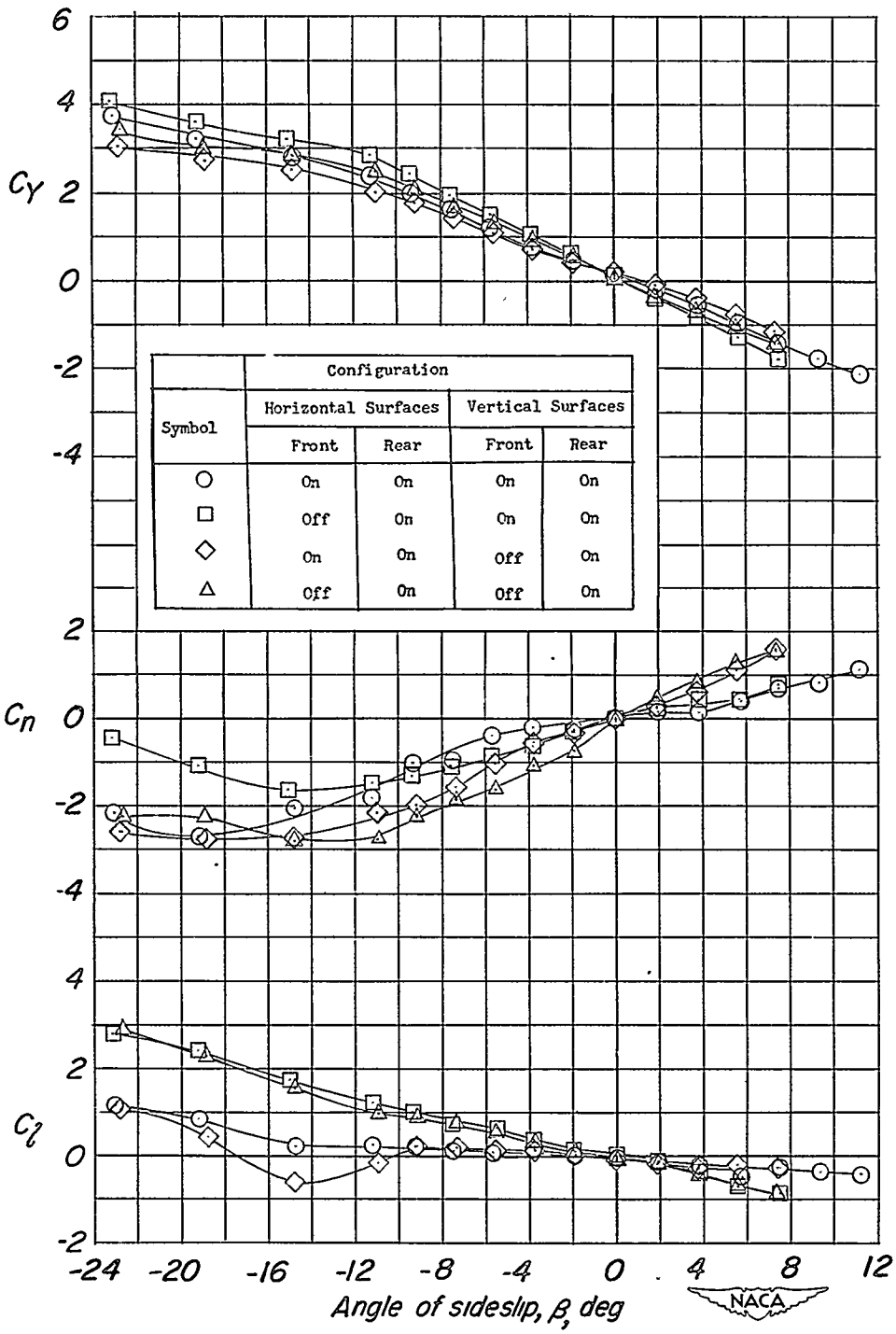

(d) $\alpha = 12^{\circ}$.

Figure 13.- Concluded.

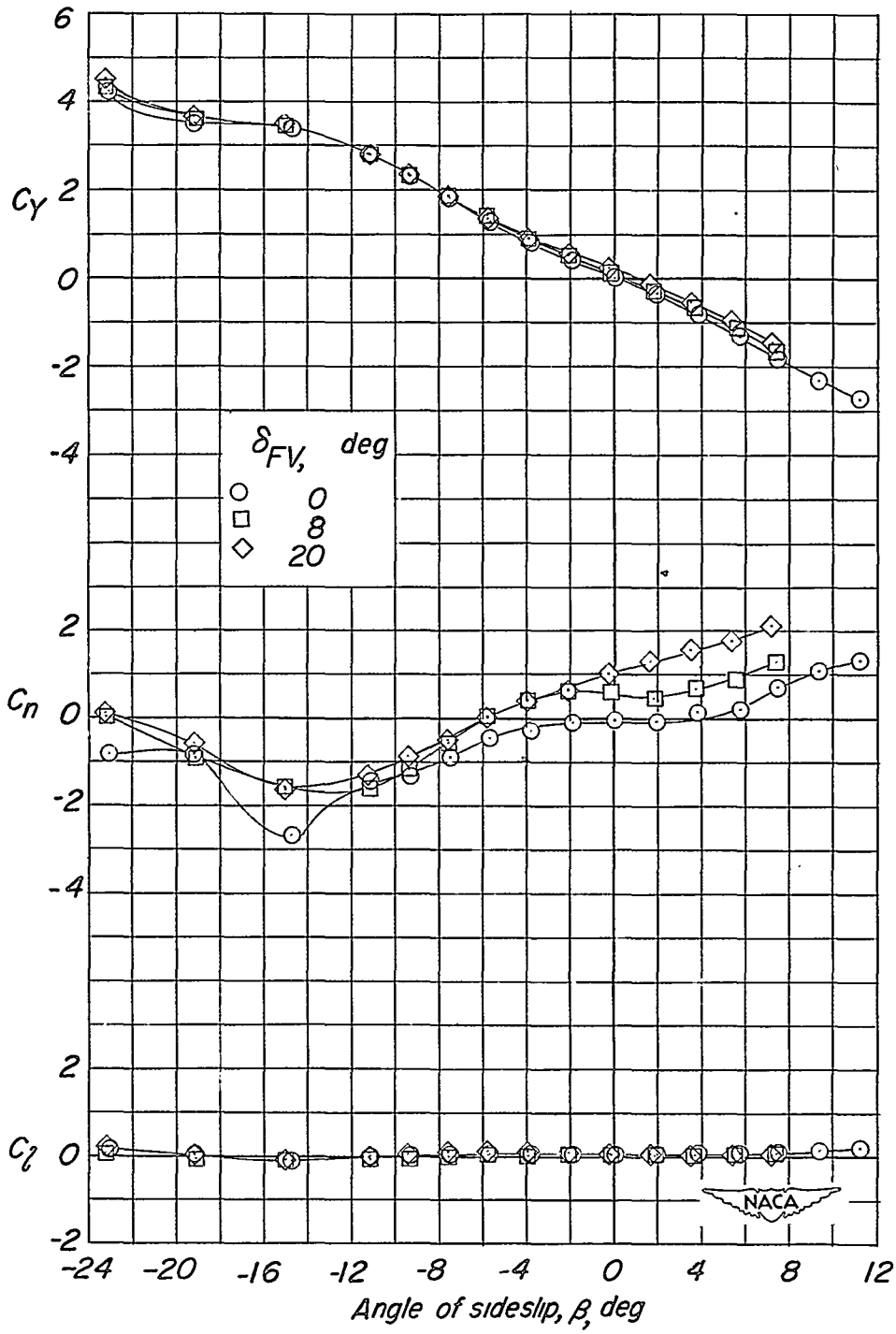

(a) $\alpha = 0^\circ$.

Figure 14.- Variation of side-force, yawing-moment, and rolling-moment coefficients with sideslip angle for model with forward vertical surfaces deflected 0°, 8°, and 20°. Complete model.

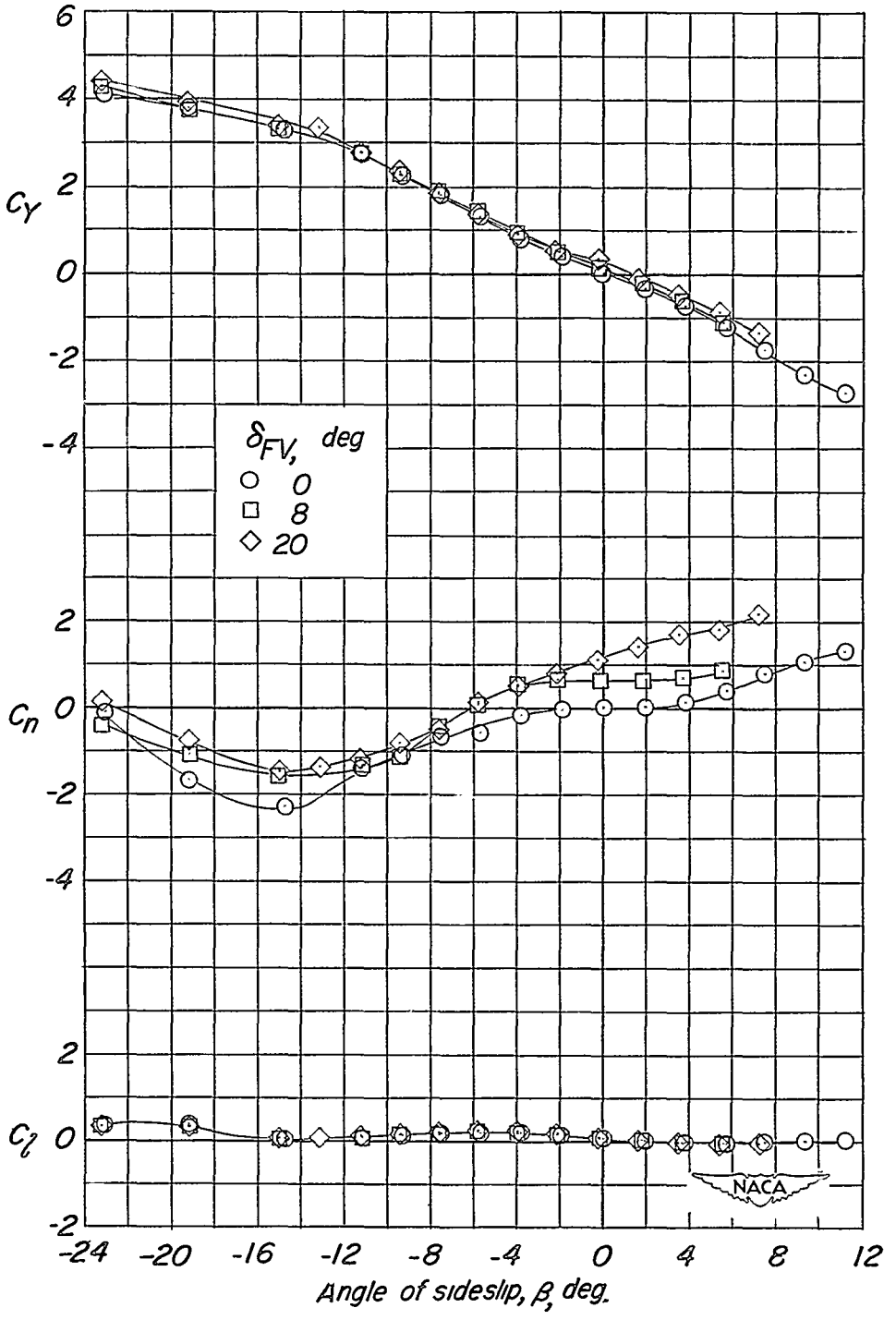

(b) $\alpha = 4^\circ$.

Figure 14.- Continued.

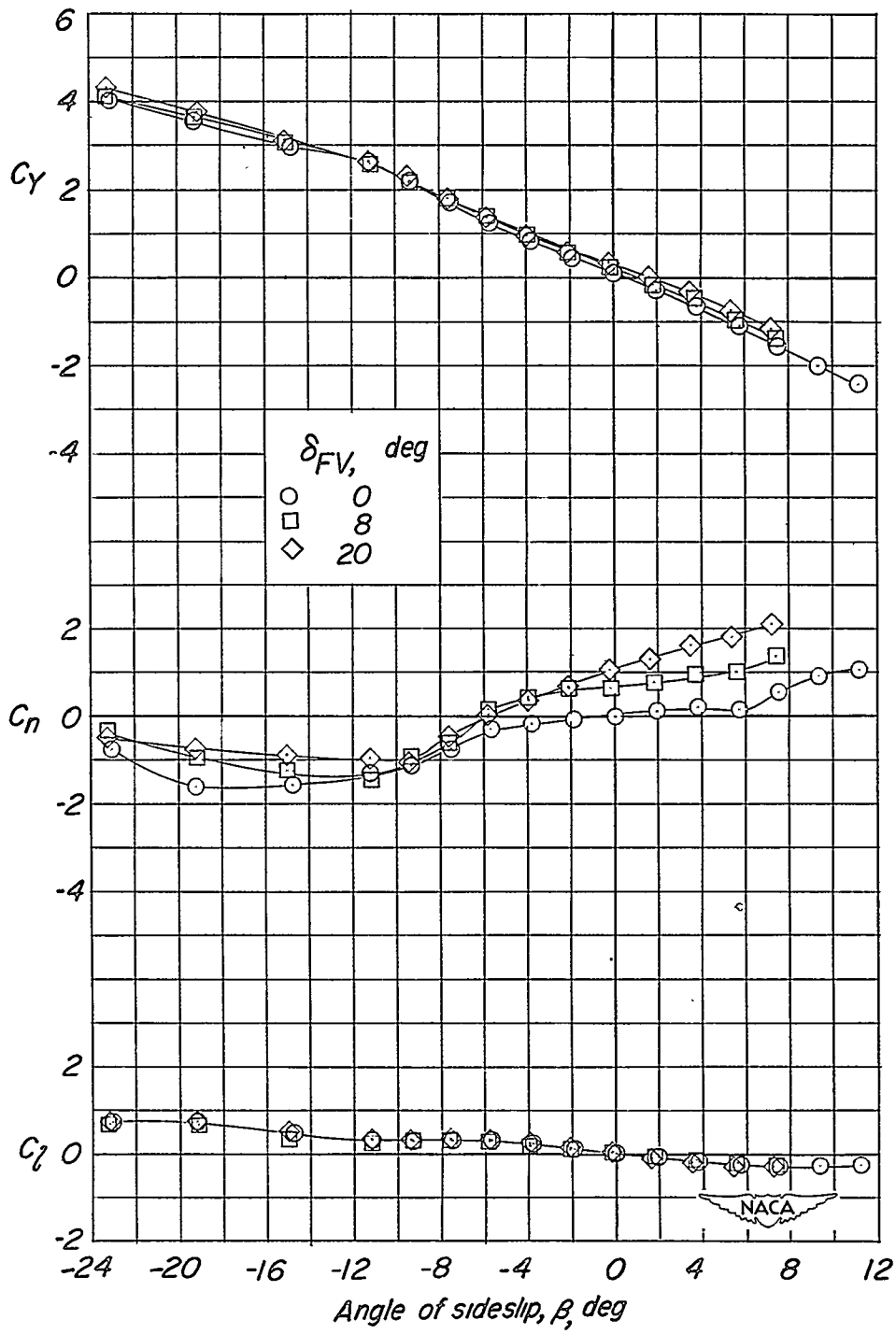

(c) $\alpha = 8^\circ$.

Figure 14.- Continued.

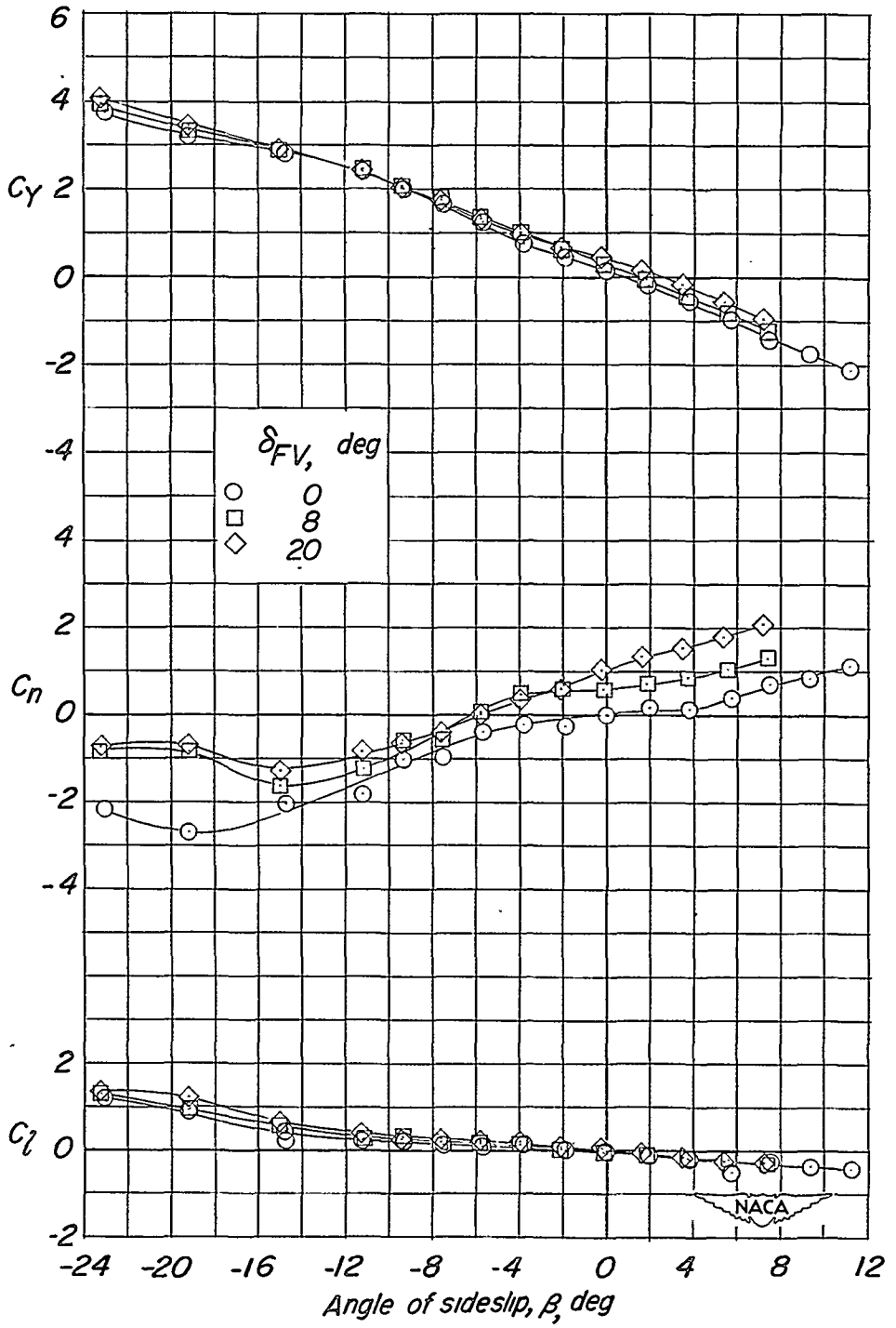

(d) $\alpha = 12^{\circ}$.

Figure 14.- Concluded.

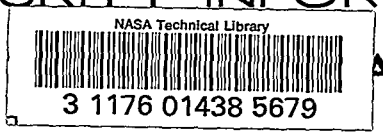

[redacted]